

On Partly Smoothness, Activity Identification and Faster Algorithms of L_1 over L_2 Minimization

Min Tao, Xiao-Ping Zhang, *Fellow, IEEE* and Zi-Hao Xia

Abstract—The L_1/L_2 norm ratio arose as a sparseness measure and attracted a considerable amount of attention due to three merits: (i) sharper approximations of L_0 compared to the L_1 ; (ii) parameter-free and scale-invariant; (iii) more attractive than L_1 under highly-coherent matrices.

In this paper, we first establish the partly smooth property of L_1 over L_2 minimization relative to an active manifold \mathcal{M} and also demonstrate its prox-regularity property. Second, we reveal that ADMM $_p$ (or ADMM $_p^+$) can identify the active manifold within a finite iterations. This discovery contributes to a deeper understanding of the optimization landscape associated with L_1 over L_2 minimization. Third, we propose a novel heuristic algorithm framework that combines ADMM $_p$ (or ADMM $_p^+$) with a globalized semismooth Newton method tailored for the active manifold \mathcal{M} . This hybrid approach leverages the strengths of both methods to enhance convergence. Finally, through extensive numerical simulations, we showcase the superiority of our heuristic algorithm over existing state-of-the-art methods for sparse recovery.

Index Terms—Sparse recovery, partly smooth, Prox-regularity, active set, nonsmooth analysis, identifiable surface

I. INTRODUCTION

In scientific and engineering domains, the primary goal is to acquire a low-dimensional representation from high-dimensional data. This objective heavily relies on the critical assumption of sparsity. Sparsity has proven to be essential in effectively addressing diverse applications across fields such as compressive sensing [1–3], machine learning [4], image processing [5, 6], and matrix factorization [7].

The use of the L_1 norm over L_2 norm in nonconvex regularized models has gained increasing attention in the field of compressive sensing [6, 8–15]. This ratio is known for its ability to promote sparsity, and exhibits desirable properties such as scale-invariance [16] and parameter-free characteristics and is much more efficient than L_1 when sensing matrix highly-coherent [17, 18]. More discussion can be found in [9, 14]. As a result, L_1/L_2 minimization has found widespread applications in various domains; see, e.g., [5, 6, 15, 19, 20].

This work of M. Tao is supported partially by the Natural Science Foundation of China (No. 11971228) and partially by Jiangsu University QingLan Project. The work of X.-P. Zhang is supported by the Natural Sciences and Engineering Research Council of Canada (NSERC), Grant No. RGPIN-2020-04661.

M. Tao is with the Department of Mathematics, National Key Laboratory for Novel Software Technology, Nanjing University, Nanjing 210093, China. Email: taom@nju.edu.cn

X.-P. Zhang is with the Department of Tsinghua-Berkeley Shenzhen Institute, Tsinghua University, Beijing, China, Department of Electrical, Computer and Biomedical Engineering, Toronto Metropolitan University, Toronto ON M5B 2K3, Canada. Email: xpzhang@ieee.org

Z.-H. Xia is with the Dept. of Mathematics, Nanjing University.

Much of the existing literature focuses on the unconstrained,

$$\min_{\mathbf{x} \in \mathcal{X}} F_u(\mathbf{x}) := \gamma \frac{\|\mathbf{x}\|_1}{\|\mathbf{x}\|_2} + \Phi(\mathbf{x}), \quad (1)$$

where $\mathcal{X} = \mathbb{R}^n/\mathbb{R}_+^n$ (resp. arbitrary signal and nonnegative signal) and the data-fitting term of $\Phi: \mathbb{R}^m \rightarrow \mathbb{R}$ differentiable and the balance parameter $\gamma > 0$. In this paper, we focus on the model (1).

The equivalence between L_1/L_2 and L_0 for signal reconstruction under different conditions has been studied by Yin et al. [9], Xu et al. [12], and Zhou and Yu [21]. However, due to the nonconvex and nonsmooth nature of L_1/L_2 minimization, finding a global solution is challenging. Consequently, various algorithms have been developed to search for stationary points. Specifically, the scaled gradient projection method (SGPM) [8, 9] has been proposed for (1) with $\mathcal{X} = \mathbb{R}_+^n$. The alternating direction method of multipliers (ADMM) [14] with double variable duplication and accelerated schemes [22] has been proposed for the following constrained model (2) with $\sigma = 0$ for noiseless data.

$$\min_{\mathbf{x} \in \mathcal{X}} F_c(\mathbf{x}) := \frac{\|\mathbf{x}\|_1}{\|\mathbf{x}\|_2} + \iota_{\{\mathbf{x}: \|A\mathbf{x} - \mathbf{b}\|_2 \leq \sigma\}}(\mathbf{x}). \quad (2)$$

The constrained model (2) aims to address the recovery from observations corrupted by Gaussian noise, where σ corresponds to the noise level. Specifically, $\sigma = 0$ indicates noise-free observations, while $\sigma > 0$ is associated with noisy data. The moving-balls-approximation-based algorithms [13] have been developed to address the constrained model (2) in both noise-free and noisy scenarios. The intricate connections between (1) and (2), we refer to [13, 23] for more discussions. For solving (1), the ADMM $_p$ [10] and ADMM $_p^+$ [11] methods have been introduced in our previous work. These approaches come with global convergence guarantees and are tailored for cases where $\mathcal{X} = \mathbb{R}^n$ and $\mathcal{X} = \mathbb{R}_+^n$, respectively. Additionally, an alternating forward-backward algorithm with a smoothing technique (SOOT) was proposed in [6] for solving blind deconvolution via L_1 over L_2 minimization.

The superiority of ADMM $_p$ and ADMM $_p^+$ has been empirically validated in the context of sparse arbitrary/nonnegative signal recovery [10, 11]. Notably, the explicit expression for all proximal points of the proximal operators of L_1/L_2 has been characterized in [10, Theorem 3.2]. Furthermore, in [10, Theorem 3.3] and [11, Theorem 6], one of the proximal points of the proximal operators L_1/L_2 (i.e., $\frac{\|\mathbf{x}\|_1}{\|\mathbf{x}\|_2}$) and $(L_1/L_2)^+$ (i.e., $\frac{\|\mathbf{x}\|_1}{\|\mathbf{x}\|_2} + \iota_{\mathbb{R}_+^n}(\mathbf{x})$), respectively, has been derived without

any dependence on unknown parameters. These characterizations have paved the way for the development of practical solvers that compute exact solutions for these L_1/L_2 proximal operators, as demonstrated in algorithms; see, e.g., [10, Algorithm 3.1] and [11, Algorithm 1].

A. Motivation

The growing scale of datasets has prompted extensive research into uncovering the inherent sparsity pattern of (1) during the early phases of iterative processes. Proximity operators have emerged as a valuable tool for detecting sparsity patterns within iterates, as highlighted in studies such as [24–27]. A prominent example is the widely used L_1 -norm. The associated proximity operator, known as soft-thresholding [28], aids in identifying the support set [26, 29] under some non-degenerate conditions. This property, referred to as the identification property, has been extensively explored in both convex and nonconvex contexts, as demonstrated in works by [30–35], and others.

It is important to clarify that the identification property does not prescribe a specific algorithm but rather outlines the fundamental properties required. Several algorithms fulfill these criteria, including projected gradient methods [36], projected Newton methods [37], and forward-backward-type methods [38]. A closely related concept is the notion of partly smoothness [39] (see Definition 2). Partly smoothness requires a function to exhibit smoothness along an active manifold while demonstrating sharp growth in directions away from that manifold. Building upon this concept, [24] demonstrated that if a C^p -partly smooth function ($p \geq 2$) (see [24, Definition 2.3]) is prox-regular (see Definition 1), the corresponding active manifold must be unique. Under non-degeneracy conditions and certain mild assumptions, [24] further established that the adopted algorithm can identify the active manifold within a finite number of steps. It is important to emphasize that partly smoothness is a property inherent to the studied problem, while the identification property is typically associated with the chosen algorithm.

In the present paper, we aim to address the following questions, “Whether the L_1/L_2 minimization have the partly smooth property?” and “Can ADMM $_p$ (or ADMM $_p^+$) identify the optimal manifold in a finite number of iterations when applied to (1)?” We answer both questions affirmatively.

B. This paper

Theoretically, we establish the partly smooth and prox-regular properties of L_1/L_2 minimization. We then prove general results for identifying the active manifold in a finite number of iterations, relaxing conditions compared to the classical result outlined in [24, Theorem 5.3].

Specifically, we extend the scope by relaxing the assumption from “the function f being C^p -partly smooth ($p \geq 2$)” as stated in [24, Theorem 5.3] to “ f being partly smooth, i.e., C^1 (see Definition 2).” Consequently, we demonstrate the identification property of ADMM $_p$ [10] and ADMM $_p^+$ [11] under relatively mild conditions.

The finite identification property signifies the existence of a specific index number K . The sequence generated by either ADMM $_p$ or ADMM $_p^+$ enters the active manifold when the iteration number goes beyond K . Once the active manifold is identified, the optimization problem transforms into a low-dimensional minimization, allowing the use of high-order algorithms tailored for low-dimensional manifolds to significantly enhance convergence speed.

Efficiency of ADMM $_p$ or ADMM $_p^+$ for sparse recovery has been well-illustrated [10, 11], outperforming existing state-of-the-art methods such as SGPM [8, 9], GIST ([40, Algorithm 1]), and monotone/nonmonotone APG [41], as well as SOOT [6]. Therefore, leveraging ADMM $_p$ or ADMM $_p^+$ as an initial phase and integrating a globalized semismooth Newton method on the active manifold will further accelerate the performance.

We clarify that the reasons for adopting a globalized semismooth Newton method are: (i) The objective function in (1) is C^1 (continuously differentiable) rather than C^2 (twice continuously differentiable) when restricted to the active manifold; (ii) There is no guarantee that the objective function remains convex when restricted to the active manifold, even if the manifold is a space.

In addition, although we know that the iterates will eventually identify the active manifold within a finite number of steps, an explicit expression for the index K (enter the active manifold) is unavailable. This prompts us to employ heuristic techniques for active manifold identification. More specifically, we introduce a two-phase heuristic acceleration framework:

- Initially, either ADMM $_p$ or ADMM $_p^+$ is employed to identify the active manifold by comparing adjacent support sets. The support sets remain unchanged over a specified number of iterations denoted as T (where $T \in \mathbb{N}_+$).
- In the second phase, we apply a globalized semismooth Newton method on the active manifold to achieve rapid convergence.

It’s worth mentioning that there is no theoretical guarantee for the heuristic strategy to identify the active manifold; however, we observe that it practically performs very well. With the identified active manifold, the semismooth Newton method is incorporated to solve a lower-dimension problem. Finally, we establish the eventual superlinear/quadratic convergence rate of the approach under some mild conditions.

We conducted extensive experiments to analyze algorithmic behaviors and compare various sparse recovery models. Our tests encompassed sparse recovery scenarios involving highly coherent compressive matrices using synthetic data, as well as real datasets. Our newly proposed heuristic acceleration algorithm demonstrated the ability to identify the active manifold within a finite number of steps. Notably, it significantly outperforms other state-of-the-art methods for L_1 over L_2 minimization problem.

C. Contribution

- 1) **Partly smoothness and prox-regularity of L_1 over L_2 .**
We prove the *partly smooth* and *prox-regular* properties

of the L_1/L_2 model (1), which are the theoretical basis for establishing the finite identification of ADMM $_p$ [10] and ADMM $_p^+$ [11].

- 2) **Support detection.** ADMM $_p$ (or ADMM $_p^+$) is shown to identify the active manifold in finite steps, known as *support detection* in compressive sensing. We relax the conditions in the classical results [24, Theorem 5.3] by replacing \mathcal{C}^p -partly smooth ($p \geq 2$) with partly smooth (i.e., \mathcal{C}^1), broadening the applicability of ADMM $_p$ (or ADMM $_p^+$) for finite identification. This expansion also clarifies our choice of the semismooth Newton method on the active manifold rather than the standard Newton algorithm.
- 3) **Fast algorithm with high accuracy.** A heuristic acceleration framework is introduced, employing ADMM $_p$ /ADMM $_p^+$ for active manifold identification and the globalized semismooth Newton method for convergence acceleration. Theoretical analysis demonstrates superlinear/quadratic convergence rates under mild conditions within the active manifold. Extensively numerical simulations verify its high-order convergence rate.

D. Organization

The rest of this paper proceeds as follows. We describe the notations and definitions in Section II and present a lemma to characterize the prox-regularity of fraction function. Section III elaborates on verifying the partly smoothness property of L_1 over L_2 minimization problem. Section IV establishes the general results for identifying the active manifold by relaxing the conditions in the classical result [24, Theorem 5.3]. Equipped with this, we validate ADMM $_p$ [10] (or ADMM $_p^+$ [11]) with the property of identifying the active manifold in finite iterations under much weaker conditions and along with non-degenerate assumption. Furthermore, we exploit sufficient conditions to ensure the non-degenerate condition. Additionally, we introduce a heuristic acceleration framework on the active manifold in Section IV to achieve a faster convergence rate for the L_1 over L_2 minimization problem. In Section V, we present extensive experiments to showcase the superior performance of our proposed heuristic acceleration framework for sparse recovery, using both synthetic and real datasets. Finally, our conclusions are presented in Section VI.

II. PRELIMINARY

The bold letter denotes the vector. x_i and $|\mathbf{x}|$ denote the i -th entry and the absolute value vector of \mathbf{x} in entrywise. $\|\mathbf{x}\|_p$ denote its p -norm (where $p = 1, 2, 1/2$). $\text{sign}(\mathbf{x})$ is defined as a vector of the same length as \mathbf{x} with its i -component equal to the set $[-1, 1]$ if $x_i = 0$; otherwise being the sign of each component of \mathbf{x} . $\text{supp}(\mathbf{x})$ denotes its support set. The notation of $\mathbb{R}_+^n/\mathbb{R}^n$ means \mathbb{R}_+^n or \mathbb{R}^n . Let \mathbf{e} and \mathbf{e}_i be the vectors with all entries equal to 1 and the i th entry equal to 1 while the others are zero, respectively. I_n is $n \times n$ identity matrix. Given a set of \mathcal{D} , $\text{co}\mathcal{D}$, \mathcal{D}^c and $\text{ri}(\mathcal{D})$ denote its convex hull, its complementary and its relative interior. If $\mathcal{D} \subseteq [n]$ ($[n] := \{1, \dots, n\}$), we use $\sharp(\mathcal{D})$ to present its cardinality. For a closed set \mathcal{S} , we use $\iota_{\mathcal{S}}(\mathbf{x})$ to denote its indicator function.

Given a matrix $A \in \mathbb{R}^{n \times n}$ or a vector $\mathbf{x} \in \mathbb{R}^n$ and an index set $\Lambda \subseteq [n]$, $A_{\Lambda, \Lambda}$, $\mathbf{x}|_{\Lambda}$ to denote $A(i, j)_{i, j \in \Lambda}$ and $\mathbf{x}(i)_{i \in \Lambda}$, respectively. $A \succ \mathbf{0}$ means positive definite, and $\lambda_{\min}(A)$ denotes the minimum eigenvalue of A . “dist” represents the distance function. A \mathcal{C}^1 function f means its gradient Lipschitz continuous. Analogously, we can define \mathcal{C}^p function ($p \geq 2$).

A set \mathcal{M} is a manifold around a point \mathbf{x} if $\mathbf{x} \in \mathcal{M}$ and there is an open set V containing \mathbf{x} such that $\mathcal{M} \cap V = \{\mathbf{x} \in V | \Phi(\mathbf{x}) = 0\}$ where the smooth function Φ has surjective derivative throughout V .

The polar cone of a set C is defined by $C^o = \{\mathbf{y} \in \mathbb{R}^n : \langle \mathbf{y}, \mathbf{x} \rangle \leq 0, \forall \mathbf{x} \in C\}$. An extended-real-valued function $f : \mathbb{R}^n \rightarrow (-\infty, +\infty]$ is said to be proper if $\text{dom}f = \{\mathbf{x} \in \mathbb{R}^n | f(\mathbf{x}) < \infty\}$ is nonempty. We denote the extended reals by $\overline{\mathbb{R}} = [-\infty, +\infty]$.

We review some definitions from [42]. Consider a function $h : \mathbb{R}^n \rightarrow \overline{\mathbb{R}}$ finite at a point $\mathbf{x} \in \mathbb{R}^n$, the subderivative $dh(\mathbf{x})(\cdot) : \mathbb{R}^n \rightarrow \overline{\mathbb{R}}$ is defined by

$$dh(\mathbf{x})(\bar{\mathbf{w}}) = \lim_{\tau \downarrow 0} \inf_{\mathbf{w} \rightarrow \bar{\mathbf{w}}} \frac{h(\mathbf{x} + \tau \mathbf{w}) - h(\mathbf{x})}{\tau},$$

and the regular subdifferential $\hat{\partial}h(\hat{\mathbf{x}})$ and the limiting subdifferential $\partial h(\hat{\mathbf{x}})$ are defined as

$$\hat{\partial}h(\hat{\mathbf{x}}) = \left\{ \mathbf{v} \left| \liminf_{\mathbf{x} \rightarrow \hat{\mathbf{x}}, \mathbf{x} \neq \hat{\mathbf{x}}} \frac{h(\mathbf{x}) - h(\hat{\mathbf{x}}) - \langle \mathbf{v}, \mathbf{x} - \hat{\mathbf{x}} \rangle}{\|\mathbf{x} - \hat{\mathbf{x}}\|_2} \geq 0 \right. \right\},$$

$$\partial h(\hat{\mathbf{x}}) = \left\{ \mathbf{v} \left| \exists \mathbf{x}^r \rightarrow \hat{\mathbf{x}}, h(\mathbf{x}^r) \rightarrow h(\hat{\mathbf{x}}), \mathbf{v}^r \in \hat{\partial}h(\mathbf{x}^r), \mathbf{v}^k \rightarrow \mathbf{v} \right. \right\},$$

respectively. The horizon subdifferential is defined by

$$\partial^\infty h(\mathbf{x}) = \left\{ \lim_{\tau} \lambda_r \mathbf{v}^r \left| \mathbf{v}^r \in \partial h(\mathbf{x}^r), \mathbf{x}^r \rightarrow \mathbf{x}, h(\mathbf{x}^r) \rightarrow h(\mathbf{x}), \lambda_r \downarrow 0 \right. \right\}.$$

Suppose that $h(\hat{\mathbf{x}})$ is finite and $\partial h(\hat{\mathbf{x}}) \neq \emptyset$, h is *regular* at $\hat{\mathbf{x}}$ if and only if h is locally lower semicontinuous at $\hat{\mathbf{x}}$ with $\partial h(\hat{\mathbf{x}}) = \hat{\partial}h(\hat{\mathbf{x}})$ and $\partial^\infty h(\hat{\mathbf{x}}) = \hat{\partial}h(\hat{\mathbf{x}})^\infty$ [42, Corollary 8.11], where $\hat{\partial}h(\hat{\mathbf{x}})^\infty$ is recession cone (in the sense of convex analysis).

Let f be a proper lower semicontinuous function, its proximal mapping defines as

$$\text{Prox}_f(\mathbf{v}) = \arg \min_{\mathbf{x}} \left\{ f(\mathbf{x}) + \frac{1}{2} \|\mathbf{x} - \mathbf{v}\|_2^2 \right\}.$$

By defining $\frac{\|\mathbf{0}\|_1}{\|\mathbf{0}\|_2} = 1$ ¹, the objective function of the following proximal operator is lower semicontinuous,

$$\text{Prox}_{\left[\frac{\|\cdot\|_1 + \iota_{\mathcal{X}}(\cdot)}{\|\cdot\|_2} \right]}(\mathbf{q}) = \arg \min_{\mathbf{x} \in \mathcal{X}} \left(\frac{\|\mathbf{x}\|_1}{\|\mathbf{x}\|_2} + \frac{\rho}{2} \|\mathbf{x} - \mathbf{q}\|_2^2 \right). \quad (3)$$

Thus, the proximal operator of $\text{Prox}_{\left[\frac{\|\cdot\|_1 + \iota_{\mathcal{X}}(\cdot)}{\|\cdot\|_2} \right]}$ is well-defined due to [42, Definition 1.22]. One of the *proximal points* for $\mathcal{X} = \mathbb{R}^n$ and \mathbb{R}_+^n has been characterized in a *closed-form* in [10, Theorem 3.3], [11, Theorem 6], respectively.

Next, we review several concepts from variational analysis.

¹For any vector $\mathbf{x} \in \mathbb{R}^n$, $\frac{\|\mathbf{x}\|_1}{\|\mathbf{x}\|_2} \geq 1$ due to Cauchy-Schwarz inequality. Another benefit of defining $\frac{\|\mathbf{0}\|_1}{\|\mathbf{0}\|_2} = 1$ is possible to exclude the stationary being zero vector. We refer the reader to [10, 11] for more discussions.

Definition 1. (Prox-regularity) [43, Definition 2.1] A function f is prox-regular at a point $\bar{\mathbf{x}}$ for a subgradient $\bar{\mathbf{v}} \in \partial f(\bar{\mathbf{x}})$ if f is finite at $\bar{\mathbf{x}}$, locally lower semi-continuous around $\bar{\mathbf{x}}$, and there exists $\rho > 0$ such that

$$f(\mathbf{x}') \geq f(\mathbf{x}) + \langle \mathbf{v}, \mathbf{x}' - \mathbf{x} \rangle - \frac{\rho}{2} \|\mathbf{x}' - \mathbf{x}\|_2^2$$

whenever \mathbf{x} and \mathbf{x}' are near $\bar{\mathbf{x}}$ with $f(\mathbf{x})$ near $f(\bar{\mathbf{x}})$ and $\mathbf{v} \in \partial f(\mathbf{x})$ is near $\bar{\mathbf{v}}$. Furthermore, f is prox-regular at $\bar{\mathbf{x}}$ if it is prox-regular at $\bar{\mathbf{x}}$ for every $\bar{\mathbf{v}} \in \partial f(\bar{\mathbf{x}})$.

The terminology ‘‘partly smooth’’ as defined in [39, Definition 2.7] differs from that presented in [24, Definition 2.3]. Notably, the difference arises from the level of smoothness of the concerned function f . While the characterization of ‘‘partly smooth’’ in [24, Definition 2.3] necessitates the function f to exhibit C^p smooth ($p \geq 2$), the criteria outlined in [39, Definition 2.7] imposes a more relaxed condition of the function f being C^1 . We adopt the latter criterion.

Definition 2. (Partly Smooth) [39, Definition 2.7] Suppose that the set $\mathcal{M} \subset \mathbb{R}^n$ contains the point \mathbf{x} . The function $f : \mathbb{R}^n \rightarrow \bar{\mathbb{R}}$ is partly smooth at \mathbf{x} relative to \mathcal{M} if \mathcal{M} is a manifold around \mathbf{x} and the following four properties hold:

- (i) **(Restricted Smoothness)** the restriction $f|_{\mathcal{M}}$ is smooth around \mathbf{x} ;
- (ii) **(Regularity)** at every point close to \mathbf{x} in \mathcal{M} , the function f is regular and has a subgradient;
- (iii) **(Normal Sharpness)** $df(\mathbf{x})(-\mathbf{w}) > -df(\mathbf{x})(\mathbf{w})$ for all nonzero directions \mathbf{w} in $N_{\mathcal{M}}(\mathbf{x})$;
- (iv) **(Subgradient Continuity)** the subdifferential map ∂f is continuous at \mathbf{x} relative to \mathcal{M} .

We say f is partly smooth relative to a set \mathcal{M} if \mathcal{M} is a manifold and f is partly smooth at each point in \mathcal{M} relative to \mathcal{M} . Property (i) ensures that f is continuous relative to \mathcal{M} , therefore the subdifferential mapping is always outer semicontinuous relative to \mathcal{M} [42, Proposition 8.7]. Thus, property (iv) can be replaced with ‘‘the subdifferential $\partial f(\mathbf{x})$ is inner semicontinuous at \mathbf{x} relative to \mathcal{M} ’’. It means that for any sequence \mathbf{x}^r in \mathcal{M} approaching \mathbf{x} and any subgradient $\mathbf{y} \in \partial f(\mathbf{x})$, there exists subgradients $\mathbf{y}^r \in \partial f(\mathbf{x}^r)$ approaching \mathbf{y} .

Below, we review the concepts of semismooth and strongly semismooth [44] and LC^1 function [45].

Definition 3. $F : \mathbb{R}^n \rightarrow \mathbb{R}$ is directionally differentiable at \mathbf{x} . We say that F is semismooth at \mathbf{x} if for any $V \in \partial F(\mathbf{x} + \mathbf{h})$,

$$F(\mathbf{x} + \mathbf{h}) - F(\mathbf{x}) - V\mathbf{h} = o(\|\mathbf{h}\|_2).$$

F is said to be strongly semismooth at \mathbf{x} if for any $V \in \partial F(\mathbf{x} + \mathbf{h})$,

$$F(\mathbf{x} + \mathbf{h}) - F(\mathbf{x}) - V\mathbf{h} = O(\|\mathbf{h}\|_2^2).$$

Definition 4. A function $f : \mathbb{R}^n \rightarrow \mathbb{R}$ is said to be an LC^1 function on an open set Ω if f is continuously differentiable on Ω , and ∇f is locally Lipschitz on Ω .

For a LC^1 function f , its gradient is locally Lipschitz on Ω ; the gradient is differentiable almost everywhere in Ω , allowing for the definition of its generalized Jacobian in Clark’s sense,

also referred to as the generalized Hessian of f [46]. We define the generalized Hessian of f at \mathbf{x} to be the set $\partial^2 f(\mathbf{x})$ of $n \times n$ matrices defined by:

$$\partial^2 f(\mathbf{x}) := \text{co}\{H \in \mathbb{R}^{n \times n} : \exists \mathbf{x}^k \rightarrow \mathbf{x} \text{ with } \nabla f \text{ differentiable at } \mathbf{x}^k \text{ and } \nabla^2 f(\mathbf{x}^k) \rightarrow H\}.$$

Note that $\partial^2 f$ is a nonempty, convex, and compact set of symmetric matrices.

We proceed to verify the following lemma, a pivotal step in establishing the prox-regularity of the fraction function.

Lemma 1. Let $f, g : \mathbb{R}^n \rightarrow (-\infty, +\infty]$ be proper lower semicontinuous functions, and finite at $\bar{\mathbf{x}} \in \mathbb{R}^n$. Suppose that f and g are locally Lipschitz continuous around $\bar{\mathbf{x}}$ and $g(\bar{\mathbf{x}}) > 0$ and f is prox-regular at the point $\bar{\mathbf{x}}$. g is strictly differentiable at $\bar{\mathbf{x}}$, and ∇g is locally Lipschitz continuous around $\bar{\mathbf{x}}$. Then, the function $\frac{f}{g}$ is prox-regular at the point $\bar{\mathbf{x}}$.

Proof. See appendix A. □

Remark 1. The significance of this lemma lies in its pivotal role in establishing the prox-regularity property of L_1 over L_2 (with or without nonnegative constraint) regularization function, which is a crucial step to establish the finite identification of $ADMM_p$ and $ADMM_p^+$.

III. PARTLY SMOOTH

In this section, we illustrate the partly smoothness of the model (1) whenever $\mathcal{X} = \mathbb{R}_+^n / \mathbb{R}^n$. To carry out a unified analysis, we denote

$$h(\mathbf{x}) = \frac{\|\mathbf{x}\|_1}{\|\mathbf{x}\|_2} + \iota_{\mathcal{X}}(\mathbf{x}). \quad (4)$$

For any vector $\mathbf{x}_0 (\neq \mathbf{0})$, we define the manifold

$$\mathcal{M}_{\mathbf{x}_0} = \{\mathbf{x} \in \mathbb{R}^n \mid \text{supp}(\mathbf{x}) = \text{supp}(\mathbf{x}_0)\}.$$

We first characterize the normal cone (normal space) to $\mathcal{M}_{\mathbf{x}_0}$.

$$N_{\mathcal{M}_{\mathbf{x}_0}}(\mathbf{x}) = \{\mathbf{w} \in \mathbb{R}^n \mid \mathbf{w}_j = 0, j \in \text{supp}(\mathbf{x}_0)\}.$$

Proposition 1. Suppose that $\Phi(\mathbf{x})$ is smooth, the objective function $F_u(\mathbf{x}) + \iota_{\mathcal{X}}(\mathbf{x})$ ($F_u(\mathbf{x})$ defined in (1)) is partly smooth at $\mathbf{x}_0 (\neq \mathbf{0})$ relative to $\mathcal{M}_{\mathbf{x}_0}$.

Proof. See appendix B. □

Remark 2. By taking $\Phi(\mathbf{x}) = \frac{1}{2} \|\mathbf{A}\mathbf{x} - \mathbf{b}\|_2^2$ in (1), the resulting model is partly smooth (i.e., the model (1.2) [10] and the model (2) [11]).

Remark 3. If $\Phi(\mathbf{x})$ is smooth except some points (the set of these irregular points denoted by \mathcal{J}). Then, the objective function F_u in (1) is partly smooth at \mathbf{x}_0 ($\mathbf{x}_0 \neq \mathbf{0}$ and $\mathbf{x}_0 \notin \mathcal{J}$) relative to $\mathcal{M}_{\mathbf{x}_0}$. For example, $\Phi(\mathbf{x}) = \|\mathbf{A}\mathbf{x} - \mathbf{b}\|_2$ and $\mathcal{J} = \{\mathbf{x} \mid \mathbf{A}\mathbf{x} - \mathbf{b} = \mathbf{0}\}$. The resulting F_u in (1) is partly smooth at \mathbf{x}_0 ($\mathbf{x}_0 \neq \mathbf{0}$ and $\mathbf{x}_0 \notin \mathcal{J}$) relative to $\mathcal{M}_{\mathbf{x}_0}$.

IV. ACTIVITY IDENTIFICATION

In [10, 11], a closed-form solution for the proximal operator of (L_1/L_2) and $(L_1/L_2)^+$ was derived in [10, Theorem 3.3] and [11, Theorem 6], respectively. Additionally, practical solvers for finding global optimizers of (3) for $\mathcal{X} = \mathbb{R}^n$ and $\mathcal{X} = \mathbb{R}_+^n$ were developed, respectively; see, e.g., [10, Algorithm 3.1] and [11, Algorithm 1]. These practical solvers have been utilized in the context of ADMM_p [10, Algorithm 4.1] and ADMM_p⁺ [11, Algorithm 2], demonstrating excellent numerical performance for solving (1) with $\Phi(\mathbf{x}) = \frac{1}{2}\|\mathbf{A}\mathbf{x} - \mathbf{b}\|_2^2$. We unify ADMM_p and ADMM_p⁺ with general Φ as follows:

$$\begin{cases} \mathbf{x}^{k+1} \in \text{Prox}_{\left[\frac{\|\cdot\|_1 + \iota_{\mathcal{X}}(\cdot)}{\|\cdot\|_2}\right]^{\beta\gamma}} \left(\mathbf{y}^k - \frac{1}{\beta} \mathbf{z}^k \right) & (5a) \\ \mathbf{y}^{k+1} = \arg \min_{\mathbf{y}} \Phi(\mathbf{y}) + \frac{\beta}{2} \left\| \mathbf{y} - \mathbf{x}^{k+1} - \frac{\mathbf{z}^k}{\beta} \right\|_2^2 & (5b) \\ \mathbf{z}^{k+1} = \mathbf{z}^k + \beta(\mathbf{x}^{k+1} - \mathbf{y}^{k+1}), & (5c) \end{cases}$$

where $\beta_\gamma = \beta/\gamma$. Our previous studies established the global convergence of (5) when $\mathcal{X} = \mathbb{R}^n$ or $\mathcal{X} = \mathbb{R}_+^n$, respectively in [10] and [11]. In this paper, we aim to show the ability of ADMM_p and ADMM_p⁺ to identify the active manifold. In doing so, we first present a unified exposition of its convergence properties for the general Φ . The proof is similar to [10, Theorem 5.4] and [11, Theorem 7]. We omit the proof here for brevity.

Theorem 1. *Let $\{\mathbf{w}^k := (\mathbf{x}^k, \mathbf{y}^k, \mathbf{z}^k)\}$ be the sequence generated by (5). If $\beta > 2L$ (L denotes the Lipschitz constant of $\nabla\Phi$), we have $\lim_{k \rightarrow \infty} \|\mathbf{y}^k - \mathbf{y}^{k+1}\|_2 = 0$.*

The global convergence of (5) is summarized below [10, 11].

Theorem 2. *Let $\{\mathbf{w}^k\}$ be the sequence generated by (5). If $A^\top \mathbf{b} \notin \mathcal{X}^o$ and $\beta > 2L$, and $\{\mathbf{x}^k\}$ is bounded, then*

- (i) *for $\mathcal{X} = \mathbb{R}^n$, $\{\mathbf{x}^k\}$ converges to a stationary point \mathbf{x}^∞ , i.e.,*

$$0 \in \gamma \left(\frac{\text{sign}(\mathbf{x}^\infty)}{r} - \frac{a}{r^3} \mathbf{x}^\infty \right) + \nabla\Phi(\mathbf{x}^\infty),$$

where $a = \|\mathbf{x}^\infty\|_1$ and $r = \|\mathbf{x}^\infty\|_2$;

- (ii) *for $\mathcal{X} = \mathbb{R}_+^n$, $\{\mathbf{x}^k\}$ converges to a d -stationary point [47, 48] of (1), i.e.,*

$$\left\langle \mathbf{x} - \mathbf{x}^\infty, \gamma \left(\frac{\mathbf{e}}{r} - \frac{a}{r^3} \mathbf{x}^\infty \right) + \nabla\Phi(\mathbf{x}^\infty) \right\rangle \geq 0, \\ \forall \mathbf{x} \in \mathcal{X}.$$

A. Finite Identification of ADMM_p and ADMM_p⁺

We elaborate on the primary findings of (5) related to the identification of the true support set within a finite steps. First, we relax the requirement of “the function f be C^p -partly smooth ($p \geq 2$)” as stated in [24, Theorem 5.3] to the condition of “the function f be partly smooth, i.e., f be C^1 ” (see Definition 2). This relaxation allows us to establish the

finite identification property of ADMM_p (or ADMM_p⁺) under more relaxed conditions.

Theorem 3. *Let the function f be partly smooth at the point $\bar{\mathbf{x}}$ relative to the manifold \mathcal{M} , and prox-regular there, with $\mathbf{0} \in \text{ri}\partial f(\bar{\mathbf{x}})$. Suppose $\mathbf{x}_k \rightarrow \bar{\mathbf{x}}$ and $f(\mathbf{x}_k) \rightarrow f(\bar{\mathbf{x}})$. Then, $\mathbf{x}_k \in \mathcal{M}$ for all large k if and only if $\text{dist}(\mathbf{0}, \partial f(\mathbf{x}_k)) \rightarrow 0$.*

Proof. See the proof to Theorem S.7 in supplementary materials. \square

Based on this, we show the finite identification property of (5).

Theorem 4. *Let $\{\mathbf{w}^k\}$ be the sequence generated by (5). Suppose that $A^\top \mathbf{b} \notin \mathcal{X}^o$, $\beta > 2L$ and $\{\mathbf{x}^k\}$ is bounded. Then, the sequence $\{\mathbf{w}^k\}$ converges to \mathbf{w}^∞ . Suppose that $\Phi(\mathbf{x})$ is C^1 and prox-regular at \mathbf{x}^∞ . If $0 \in \text{ri}(\partial(F_u(\cdot) + \iota_{\mathcal{X}}(\cdot))(\mathbf{x}^\infty))$,*

$$\mathbf{x}_k \in \mathcal{M}_{\mathbf{x}^\infty}, \text{ for all large } k.$$

Proof. See appendix C. \square

To this end, we further exploit the condition of

$$0 \in \text{ri}(\partial(F_u(\cdot) + \iota_{\mathcal{X}}(\cdot))(\mathbf{x}^\infty)).$$

We can characterize it by dividing it into two cases:

- (a) When $\mathcal{X} = \mathbb{R}^n$,

$$0 \in \text{ri}(\partial(F_u(\cdot) + \iota_{\mathcal{X}}(\cdot))(\mathbf{x}^\infty)) \\ \Leftrightarrow \gamma \left(\frac{\text{sign}((\mathbf{x}^\infty)_\Lambda)}{r} - \frac{a}{r^3} (\mathbf{x}^\infty)_\Lambda \right) + (\mathbf{q}^\infty)_\Lambda = 0, \\ \text{and } \|(\mathbf{q}^\infty)_{\Lambda^c}\|_\infty < \gamma/r,$$

where $\mathbf{q}^\infty = \nabla\Phi(\mathbf{x}^\infty)$, $a = \|\mathbf{x}^\infty\|_1$, and $r = \|\mathbf{x}^\infty\|_2$.

- (b) When $\mathcal{X} = \mathbb{R}_+^n$,

$$0 \in \text{ri}(\partial(F_u(\cdot) + \iota_{\mathcal{X}}(\cdot))(\mathbf{x}^\infty)) \\ \Leftrightarrow \gamma \left(\frac{\mathbf{e}}{r} - \frac{a}{r^3} (\mathbf{x}^\infty)_\Lambda \right) + (\mathbf{q}^\infty)_\Lambda = 0, \\ \text{and } (\mathbf{q}^\infty)_{\Lambda^c} + \frac{\gamma}{r} > 0,$$

where \mathbf{q}^∞ , a , and r are defined the same as in Case (a).

Remark 4. *Thus, we establish the identification property of both ADMM_p and ADMM_p⁺. This property implies the existence of an index number, denoted as K , such that the sequence $\{\mathbf{x}^k\}$ generated by either ADMM_p or ADMM_p⁺ will eventually enter the active manifold. This serves as the theoretical basis for designing an acceleration framework provided in Section IV-B.*

B. Heuristic Acceleration Framework

As proven in Theorem 4, both ADMM_p and ADMM_p⁺ can successfully identify the active manifold within a finite number of iterations. To leverage this result, we develop a heuristic acceleration framework for the active manifold (abbr. HAFAM). This heuristic framework comprises two phases: (I) Utilize ADMM_p or ADMM_p⁺ to identify the active manifold; (II) Employ a globalized semismooth Newton method (abbr. **SSNewton**) to solve the reduced low-dimensional minimization problem.

Algorithm 1 Heuristic Acceleration Framework on Active Manifold (HAFAM)

Require: $A \in \mathbb{R}^{m \times n}$, $\mathbf{b} \in \mathbb{R}^m$, $\mathbf{x}_0 \in \mathbb{R}^n$, $\beta > 0$, $\tau \geq 0$, $\gamma > 0$, $T \in \mathbb{N}$.

- 1: **Phase I: Identify the active manifold by ADMM_p (or ADMM_p⁺).**
 - 2: Initialize: $\mathbf{y}^0 = \mathbf{z}^0 = \mathbf{x}_0$.
 - 3: **while** (6) not satisfied. **do**
 - 4: Solve \mathbf{x}^{k+1} via (5a).
 - 5: Compute \mathbf{y}^{k+1} via (5b).
 - 6: Update \mathbf{z}^{k+1} via (5c).
 - 7: **end while**
 - 8: Output \mathbf{x}^I .
 - 9: Compute $\widehat{\mathbf{x}} = \text{HARD}(\mathbf{x}^I, \tau)$.
 - 10: Let $\widehat{\mathcal{M}}$ be defined in (7).
 - 11: **Phase II: Globalized semismooth Newton method.**
 - 12: Use Algorithm 2 to solve (9), and
 - 13: let $\mathbf{u} = \text{SSNewton}(\widehat{\mathbf{x}}, \widehat{\mathcal{M}})$.
 - 14: Output $\bar{\mathbf{x}}$ such that $\bar{\mathbf{x}}|_{\widehat{\mathcal{M}}} = \mathbf{u}$ and $\bar{\mathbf{x}}|_{\widehat{\mathcal{M}}^c} = \mathbf{0}$.
-

The primary advantage of this approach lies in the dimension of the identified manifold, which is typically much smaller than the original. For implementation details of HAFAM, refer to Algorithm 1. Additionally, for Phase II in HAFAM, consult Algorithm 2.

To determine the transition from Phase I to Phase II, we utilize a heuristic strategy, ensuring the support set remains unchanged for consecutive T iterations. Mathematically,

$$\Lambda_k = \Lambda_{k+1} = \dots = \Lambda_{k+T}, \quad (\Lambda_k = \text{supp}(\mathbf{x}^{(k)})). \quad (6)$$

To elucidate Phase II, let \mathbf{x}^I be generated by ADMM_p or ADMM_p⁺ (5) such that (6) is satisfied. Denote $\widehat{\Lambda} = \text{supp}(\widehat{\mathbf{x}})$, and define

$$\widehat{\mathcal{M}} = \{\mathbf{x} \in \mathbb{R}^n \mid \text{supp}(\mathbf{x}) = \widehat{\Lambda}\}. \quad (7)$$

Below, we focus on $\mathcal{X} = \mathbb{R}^n$ for brevity.

Without loss of generality, we assume

$$(\mathbf{x})^\top = ((\mathbf{x}_{\widehat{\Lambda}})^\top, (\mathbf{0})^\top)$$

for any $\mathbf{x} \in \widehat{\mathcal{M}}$. Therefore, we can characterize the objective function of (1) as $\varphi: \mathbb{R}^s \rightarrow \mathbb{R}$ (let $\mathbf{u} = \mathbf{x}_{\widehat{\Lambda}}$, $s = \text{dim}(\mathbf{u})$),

$$\varphi(\mathbf{u}) = F_u \begin{pmatrix} \mathbf{u} \\ \mathbf{0} \end{pmatrix}. \quad (8)$$

Thus, the original problem (1) is transformed into an equivalent problem within a lower-dimensional space:

$$\min_{\mathbf{u} \in \mathbb{R}^s} \varphi(\mathbf{u}). \quad (9)$$

Phase II aims to solve the problem (9).

If $\Phi(\cdot)$ is LC¹-function, we calculate

$$\nabla \varphi(\mathbf{u}) = \gamma \left(\frac{\text{sign } \mathbf{u}}{\|\mathbf{u}\|_2} - \frac{\|\mathbf{u}\|_1}{\|\mathbf{u}\|_2^3} \mathbf{u} \right) + \nabla_{\mathbf{u}} \Phi \begin{pmatrix} \mathbf{u} \\ \mathbf{0} \end{pmatrix}, \quad (10)$$

Algorithm 2 SSNewton($\mathbf{x}^0, \mathcal{M}$)

1: Initialization: $\mathbf{u}^0 = \mathbf{x}^0|_{\mathcal{M}} \in \mathbb{R}^m$, $\mu \in (0, 1/2)$, $\eta, \nu \in (0, 1)$ and $\delta \in (0, 1)$. Define φ and $\nabla \varphi$ by (8), (10), respectively.

2: **while** “not converge” **do**

3: Let $V_j \in \partial^2 \varphi(\mathbf{u}^j)$. Find an approximate solution \mathbf{d}^j to

$$V_j \mathbf{d}^j = -\nabla \varphi(\mathbf{u}^j), \quad (12)$$

4: such that

$$\|\nabla \varphi(\mathbf{u}^j) + V_j \mathbf{d}^j\|_2 \leq \eta_j \|\nabla \varphi(\mathbf{u}^j)\|_2, \quad (13)$$

5: where $\eta_j = \min\{\eta, \|\nabla \varphi(\mathbf{u}^j)\|_2\}$.

6: **if** (13) is unachievable or $\langle \nabla \varphi(\mathbf{x}^j), \mathbf{d}^j \rangle > -\nu_j \|\mathbf{d}^j\|_2^2$

then

7: $\mathbf{d}^j = -B_j^{-1} \nabla \varphi(\mathbf{d}^j)$.

8: **end if**

9: where $\nu_j = \min\{\nu, \|\varphi(\mathbf{u}^j)\|_2\}$ and $B_j \succ \mathbf{0}$.

10: **for** $m = 0, 1, 2, \dots$ **do**

11: Set $\alpha_j = \delta^m$,

12: **if** α_j satisfies

13: $\varphi(\mathbf{u}^j + \alpha_j \mathbf{d}^j) \leq \varphi(\mathbf{u}^j) + \mu \alpha_j \langle \nabla \varphi(\mathbf{u}^j), \mathbf{d}^j \rangle$.

14: Set $\mathbf{u}^{j+1} = \mathbf{u}^j + \alpha_j \mathbf{d}^j$.

15: **end for**

16: **end while**

17: Output \mathbf{u} .

and the generalized Hessian of φ

$$\begin{aligned} \partial^2 \varphi(\mathbf{u}) = \{ \mathcal{V} \mid \mathcal{V} = V_{\widehat{\Lambda}, \widehat{\Lambda}} \\ - \gamma \frac{1}{r^2} \left(\frac{\mathbf{u}(\text{sign}(\mathbf{u}))^\top + \text{sign}(\mathbf{u})\mathbf{u}^\top}{r} \right) + \gamma \frac{3a\mathbf{u}\mathbf{u}^\top}{r^5} - \gamma \frac{a}{r^3} \}, \end{aligned} \quad (11)$$

where $V \in \partial^2 \Phi(\mathbf{x})$, and $a = \|\mathbf{u}\|_1$ and $r = \|\mathbf{u}\|_2$. By defining

$$Q = \frac{\gamma}{r^3} \left[(\mathbf{u}(\text{sign}(\mathbf{u}))^\top + \text{sign}(\mathbf{u})\mathbf{u}^\top) - \frac{3a\mathbf{u}\mathbf{u}^\top}{r^2} + aI \right],$$

we can show that all the eigenvalues of Q are as follows:

$$\lambda_1 = \frac{\gamma(a - \sqrt{4sr^2 - 3a^2})}{2r^3}, \quad \lambda_2 = \frac{\gamma(a + \sqrt{4sr^2 - 3a^2})}{2r^3},$$

accompanied with 0 eigenvalue in the multiplicity of $s - 2$. Obviously, $\lambda_1 < 0$ and $\lambda_2 > 0$.

With these preparatory results, the globally semismooth Newton method can be applied to solve (9), and more details can be found in Algorithm 2.

Except the two phases in Algorithm 1, there is an additional hard-shrinkage step, and the operator HARD is defined as:

$$\text{HARD}(\mathbf{x}, \tau) = \max(|\mathbf{x}| - \tau, 0) .* \mathbf{x},$$

where $.*$ denotes componentwise multiplication. This step is to address the recovery under noisy data. More specifically, we set $\tau = 0$ when the data is noiseless and $\tau > 0$ when the observation is noisy.

Remark 5. In Algorithm 2, we practically use the conjugate gradient (CG) method to solve the following perturbed Newton equation:

$$(V_j + \varepsilon_k I) \mathbf{d}^j + \nabla \varphi(\mathbf{u}^j) = 0,$$

where $\varepsilon_k = \|\varphi(\mathbf{u}^j)\|_2$.

Remark 6. In Algorithm 2, the matrix B_j is any real symmetric positive definite matrix for all j .

C. High-Order Convergence Guarantees

We establish the proposed approach's eventual superlinear/quadratic convergence rate under the assumption that the objective function possesses a smooth representation that is semismooth/strongly semismooth, along with some additional conditions. The analysis of the following theorem is inspired by [49, Theorem 5.3] and [50]. For the sake of completeness, we have included the proof here.

Theorem 5. Suppose the assumptions in Theorem 4 are fulfilled and $\Phi(\mathbf{x})$ is LC^1 and bounded below. Both $\{\|B_j\|_2\}$ and $\{\|B_j^{-1}\|_2\}$ are uniformly bounded. Let $\{\mathbf{u}^j\}$ be generated by Algorithm 2 with $\mathcal{M} = \mathcal{M}_{\mathbf{x}^\infty}$.

- (i) Any accumulation point $\hat{\mathbf{u}}$ of $\{\mathbf{u}^j\}$ is a critical point of (9).
- (ii) Furthermore, assume that φ is level bounded on $\mathcal{M}_{\mathbf{x}^\infty}$. If $\nabla \varphi$ is semismooth at $\hat{\mathbf{u}}$ and for all $\hat{V} \in \partial^2 \varphi(\hat{\mathbf{u}})$ are positive definite, then the whole sequence $\{\mathbf{u}^j\}$ converges to $\hat{\mathbf{u}}$ superlinearly; if $\nabla \varphi$ is strongly semismooth at $\hat{\mathbf{x}}$, then the sequence $\{\mathbf{u}^j\}$ converges to $\hat{\mathbf{u}}$ quadratically.
- (iii) By defining $\hat{\mathbf{x}}|_{\hat{\Lambda}} = \hat{\mathbf{u}}$ and $\hat{\mathbf{x}}|_{\hat{\Lambda}^c} = \mathbf{0}$, $\hat{\mathbf{x}}$ recovers a critical point of (1).

Proof. See appendix D. \square

Remark 7. Suppose $V_{\hat{\Lambda}, \hat{\Lambda}} \succ \mathbf{0}$ defined in (11) with $\mathbf{u} = \hat{\mathbf{u}}$. There exists a scalar $\bar{\gamma} > 0$ (e.g., $\bar{\gamma} = \frac{2\|\hat{\mathbf{u}}\|_2 \lambda_{\min}(V_{\hat{\Lambda}, \hat{\Lambda}})}{3\sqrt{\|\hat{\mathbf{u}}\|_0}}$) such that when $0 < \gamma < \bar{\gamma}$, then all the $\hat{V} \in \partial^2 \varphi(\hat{\mathbf{u}})$ are positive definite.

V. NUMERICAL RESULTS

We present numerical results to illustrate the efficiency of the proposed algorithmic framework (i.e., Algorithm 1) and its ability to achieve high-order convergence rates and high-accuracy solutions. The efficiency of ADMM_p/ADMM_p⁺ for arbitrary/nonnegative sparse recovery has been well demonstrated in [10, 11] in comparison with the existing state-of-the-art methods. Below, we focus on the comparisons between Algorithm 1 and ADMM_p. All these algorithms are implemented on MATLAB R2016a, and performed on a desktop with Windows 10 and an Intel Core i7-7600U CPU processor (2.80GH) with 16GB memory. The stopping criterion of ADMM_p we adopt relative error (RelErr) less than a threshold:

$$\text{RelErr} = \frac{\|\mathbf{x}^{k-1} - \mathbf{x}^k\|_2}{\max\{10^{-16}, \|\mathbf{x}^k\|_2, \|\mathbf{x}^{k-1}\|_2\}} < 10^{-8}$$

or $k_{\max} > \text{IMax}$. (14)

Let $\text{IMax} = 2000$. Set $T = 5, 10, 20, 30$ in Algorithm 1, denoted as HAFAM_T. The setting of parameter β in HAFAM_T is the same as ADMM_p. For SSNewton($\hat{\mathbf{x}}, \hat{\mathcal{M}}$), we take $\eta = 1e - 3$, $\nu = 1e - 8$, $\mu = 1e - 8$, $\delta = 0.95$ and $B_j = 0.1I$ for all j . We used

$$\|\nabla \varphi(\mathbf{u}^j)\|_2 \leq 1e - 11 \quad \text{or } j > \text{SSNMax}$$

as the termination criterion and $\text{SSNMax} = 2500$.

To measure the similarity degree between the support sets of two vectors, we introduce the *identification accuracy* (IAcc) function. Given two vectors $\mathbf{x}^{(1)}, \mathbf{x}^{(2)} \in \mathbb{R}^n$, we define

$$\text{IAcc}(\mathbf{x}^{(1)}, \mathbf{x}^{(2)}) = \frac{1}{n} \sum_{i=1}^n \delta(\mathbf{x}_i^{(1)}, \mathbf{x}_i^{(2)})$$

where $\delta(\mathbf{x}_i^{(1)}, \mathbf{x}_i^{(2)}) = 1$ if both $\mathbf{x}_i^{(1)}$ and $\mathbf{x}_i^{(2)}$ are either zero or nonzero; otherwise, $\delta(\mathbf{x}_i^{(1)}, \mathbf{x}_i^{(2)}) = 0$. Obviously, $\text{IAcc}(\mathbf{x}^{(1)}, \mathbf{x}^{(2)}) = \text{IAcc}(\mathbf{x}^{(2)}, \mathbf{x}^{(1)})$ and $0 \leq \text{IAcc}(\mathbf{x}^{(1)}, \mathbf{x}^{(2)}) \leq 1$. A larger IAcc value signifies higher accuracy in the identification. Clearly, $\text{IAcc}(\mathbf{x}^{(1)}, \mathbf{x}^{(2)}) = 1$ if and only if $\text{supp}(\mathbf{x}^{(1)}) = \text{supp}(\mathbf{x}^{(2)})$.

To measure the extent of satisfying optimality condition of (1), we define the Karush-Kuhn-Tucker residual on the support set (KKT_R) of the last iterate \mathbf{x} as:

$$\text{KKT}_R = \left\| \gamma \left(\frac{\text{sign}(\mathbf{x}_\Lambda)}{\|\mathbf{x}\|_2} - \frac{\|\mathbf{x}\|_1}{\|\mathbf{x}\|_2^3} \mathbf{x}_\Lambda \right) + (A_\Lambda)^\top (A\mathbf{x} - \mathbf{b}) \right\|_2,$$

where $\Lambda = \text{supp}(\mathbf{x})$.

A. Sparse Recovery

We focus on the sparse recovery by solving (1) with $\Phi(\mathbf{x}) = \frac{1}{2} \|A\mathbf{x} - \mathbf{b}\|_2^2$ and $A \in \mathbb{R}^{m \times n}$ ($m \ll n$), $\mathbf{b} \in \mathbb{R}^m$. Two types of sensing matrices are considered: (I) Gaussian matrix. A is subject to $\mathcal{N}(\mathbf{0}, \Sigma)$ with $\Sigma = ((1-r)I_n + r)$ with $r \in (0, 1)$. (II) Oversampled DCT (O-DCT). $A = [\mathbf{a}_1, \mathbf{a}_2, \dots, \mathbf{a}_n] \in \mathbb{R}^{m \times n}$ with each column $\mathbf{a}_j = \frac{1}{\sqrt{m}} \cos\left(\frac{2\pi \mathbf{w} j}{F}\right)$ ($j = 1, \dots, n$), where $\mathbf{w} \in \mathbb{R}^m$ is a uniformly distribution on $[0, 1]$ random vector and $F \in \mathbb{R}_+$ controls the coherence. We generate an s -sparse ground truth signal $\mathbf{x}^* \in \mathbb{R}^n$ with dynamic range $(\text{sign}(\text{randn}(K, 1))) * 10^D * \text{randn}(K, 1)$ in matlab script) and D is specified later.

First, we test two types of matrices (Gaussian matrix, O-DCT) with the ground-truth having sparsity $s = 12$, where nonzero entries are generated by dynamic range with $D = 1$. We generate $\mathbf{b} = A\mathbf{x}^*$. The size of the sensing matrix (m, n) is 256×2048 . We set $\gamma = 0.0001$ in (1) and $\beta = 0.015$ in ADMM_p.

In Fig. 1, we depict the evolution of $\text{RErr} \left(\frac{\|\mathbf{x}^k - \mathbf{x}^*\|_2}{\|\mathbf{x}^*\|_2} \right)$ and KKT_R over iterations for ADMM_p and HAFAM_T with different values of T (i.e., $T = 5, 10, 20, 30$). The results are presented separately for the cases of Gaussian matrices (top row) and O-DCT matrices (bottom row). Notably, it is evident that the convergence of HAFAM_T (particularly with $T = 5$) is significantly faster compared to ADMM_p. The RErr and KKT_R values consistently exhibit a linear reduction, leading to the attainment of the lowest values. This accelerated convergence process stands out as a significant advantage of HAFAM_T.

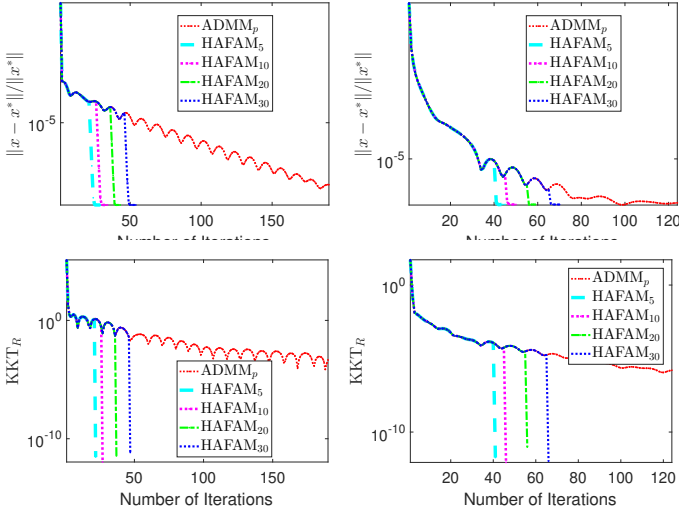


Fig. 1. Comparison between ADMM_p and HAFAM_T ($T = 5, 10, 20, 30$) for Gaussian matrices with $r = 0.8$ (top row) and O-DCT matrices with $F = 10$ (bottom row). The evolution of RErr and KKT_R from HAFAM_T consistently exhibits a linear reduction when the active manifold is identified, highlighting its accelerated convergence over ADMM_p .

TABLE I
RESULTS ON ADMM_p AND HAFAM_T

Algo.	AD_p	HA_5	HA_{10}	HA_{20}	HA_{30}
RErr	4.45e-08	7.59e-09	7.59e-09	7.59e-09	7.59e-09
CPU	3.58e-01	5.27e-02	5.71e-02	9.19e-02	9.68e-02
Obj	2.99e-04	2.99e-04	2.99e-04	2.99e-04	2.99e-04
KKT_R	4.55e-04	3.09e-12	1.07e-12	3.39e-12	7.08e-12
TranIt	—	21	26	36	46
ToIt	190	30	35	44	55
IAcc1	1	1	1	1	1

In Table I, we present the outcomes of ADMM_p (AD_p) and HAFAM_T (HA_T) concerning the Gaussian matrix scenario in terms of RErr , computational time in seconds (CPU), final objective function value (Obj), KKT_R , the iteration number of transferring to SSNewton (TranIt), total iteration number (ToIt), $\text{IAcc}(\mathbf{x}^I, \tilde{\mathbf{x}})$ (IAcc1). Here, \mathbf{x}^I represents the iterate from HAFAM_T when the heuristic strategy (6) is satisfied. $\tilde{\mathbf{x}}$ corresponds to the last iterate from ADMM_p until the stopping criterion (14) is satisfied. The data in Table I illustrates that HAFAM_T identifies the active manifold (i.e., the true support set) within a finite number of iterations for all tested T , as indicated by the values of IAcc1 being all 1. Notably, ADMM_p also achieves this within a finite iteration, as the first phase in HAFAM_T is essentially ADMM_p .

In the second part, we perform a performance profiles [51] for ADMM_p and HAFAM_T ($T = 5, 10, 20, 30$) in terms of KKT_R and CPU. The analysis involves 90 different problems with Gaussian matrices ($r = 0.7, 0.8, 0.9$) and O-DCT matrices ($F = 5, 10, 15$), varying sparsity ($s = 4 : 2 : 32$), and dimensions $(m, n) = (64, 1024)$. Nonzero entries of the ground truth are generated with dynamic range using $D = 2$.

Let $t_{p,j}$ denote a performance metric (lower are preferable) for the j th solver on problem p . We calculate the ratio $r_{p,j}$ by dividing $t_{p,j}$ by the smallest value achieved by any of the j solvers for problem p , i.e., $r_{p,j} = \frac{t_{p,j}}{\min\{t_{p,j}: 1 \leq j \leq n_j\}}$. For a

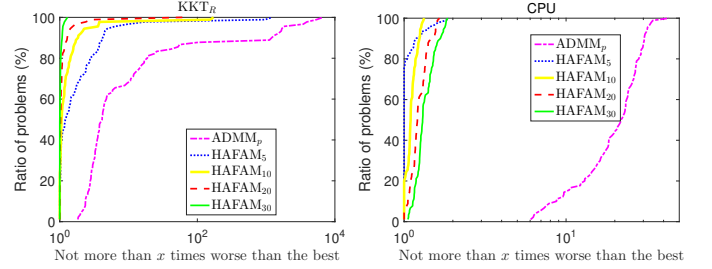


Fig. 2. The performance profiles of ADMM_p and HAFAM_T ($T = 5, 10, 20, 30$) for 90 different problems. HAFAM_{30} excels in KKT_R performance among these comparing algorithms, while HAFAM_5 takes the least CPU time.

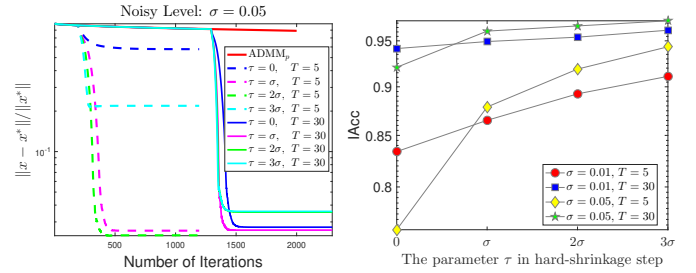


Fig. 3. The evolution of the RErr from ADMM_p and HAFAM_T ($T = 5, 30$) with varying τ values under a noise level of $\sigma = 0.05$ (left) and the $\text{IAcc}(\mathbf{x}^I, \mathbf{x}^*)$ values for different τ settings under two noise levels (right). Specifically, the values of $\text{IAcc}(\mathbf{x}^I, \mathbf{x}^*)$ for $\tau = 0, \sigma, 2\sigma, 3\sigma$ are provided: (a) [$\sigma = 0.01, T = 5$]: 0.83, 0.87, 0.89, 0.91; (b) [$\sigma = 0.01, T = 30$]: 0.94, 0.95, 0.95, 0.96; (c) [$\sigma = 0.05, T = 5$]: 0.76, 0.88, 0.92, 0.94; (d) [$\sigma = 0.05, T = 30$]: 0.92, 0.96, 0.97, 0.97.

given threshold $\tau > 0$, $\pi_j(\tau)$ is the ratio of the number of problems where $r_{p,j} \leq \tau$ to the total number. This provides insight into whether solver j performs within a factor of τ in comparison to the best-performing solver.

Fig. 2 presents the performance profiles of KKT_R and CPU. It shows that KKT_R of HAFAM_{30} is better than the others on all the problems while CPU time of HAFAM_5 are less than the others on the most problems. A similar phenomenon is also observed for RErr , we omit the corresponding plot for conciseness.

In summary, Phase I of Algorithm 1 is dedicated to identifying the active manifold, and Phase II focuses on accelerating the convergence rate within the dimension-reduced space. The introduction of the hard-shrinkage step (Line 9) in Algorithm 1 is specifically to address the noisy data.

To empirically substantiate this, we conduct a case study for the model (1) with $\Phi(\mathbf{x}) = \frac{1}{2} \|\mathbf{A}\mathbf{x} - \mathbf{b}\|_2^2$. The matrix $\mathbf{A} \in \mathbb{R}^{64 \times 1024}$ is O-DCT, and the ground truth $\mathbf{x}^* \in \mathbb{R}^{1024}$ has sparsity $s = 6$ and a dynamic range $D = 1$. We generate $\mathbf{b} = \mathbf{A}\mathbf{x}^* + \varepsilon$, where the noise ε follows a normal distribution $N(\mathbf{0}, \sigma)$, with two noise levels: (a) $\sigma = 0.01$ and (b) $\sigma = 0.05$.

The evolution of RErr over iterations is provided in Fig. 3 (left plot) for the case $\sigma = 0.05$. We present results for ADMM_p and HAFAM_T with $T = 5, 30$, both with and without the hard-shrinkage step, corresponding to $\tau = \sigma, 2\sigma, 3\sigma$, and $\tau = 0$. Notably, the inclusion of the hard-shrinkage step in HAFAM_5 at $\tau = 2\sigma$ outperforms the others, demonstrating the lowest RErr . As $T = 30$, the performance gap between with

and without the hard-shrinkage step diminishes compared to $T = 5$.

Additionally, we compute the value of $\text{IAcc}(\mathbf{x}^I, \mathbf{x}^*)$, where \mathbf{x}^I represents the iterate from HAFAM_T satisfying (6), and \mathbf{x}^* is the ground truth. The results are plotted in Fig. 3 (right plot). We observe an increase in the accuracy of identifying the true support set when incorporating the hard-shrinkage step under both noisy levels.

B. Validation of finite identification

We conduct the numerical validations for the finite identification property of ADMM_p and focus on (1) with $\Phi(\mathbf{x}) = \frac{1}{2}\|\mathbf{A}\mathbf{x} - \mathbf{b}\|_2^2$.

We test on Gaussian matrix A with $r = 0.8$. The dimensions of the sensing matrix (m, n) are fixed at $n = 1024$, with $m = 16 : 16 : 256$. We generate an s -sparse ground truth signal $\mathbf{x}^* \in \mathbb{R}^n$ with dynamic range with $D = 1$ and let the sparsity $s = 1 : 1 : 16$. This results in a total of 256 distinct problem instances.

For each of the 256 distinct problems, we execute ADMM_p until (14) is satisfied, recording the final iterate as $\hat{\mathbf{x}}$. Subsequently, we apply HAFAM_T ($T = 5, 10, 20, 30$) until reaching the iterate that satisfies (6), denoted as \mathbf{x}_T^I (with the subscript T to differentiate different HAFAM_T). For each scenario, 50 random instances are generated, and the average $\text{IAcc}(\hat{\mathbf{x}}, \mathbf{x}_T^I)$ is computed. The results are illustrated in Fig. 4, where the x -axis and y -axis represent ratios of s/m and $m/256$, respectively.

As observed in Fig. 4, the value of $\text{IAcc}(\hat{\mathbf{x}}, \mathbf{x}_T^I)$ consistently increases with the growth of T , ranging between 0.98 and 1. This indicates that running HAFAM_T until it satisfies (6) can identify the support set (i.e., active manifold). It also implies that ADMM_p can identify the active manifold within a finite number of iterations.

C. Realistic Dataset

We verify the superiority of the proposed algorithm (HAFAM_T) in comparison with ADMM_p through L_1/L_2 model (1) with two types of data fidelity term $\Phi(\mathbf{x}) = \frac{1}{2}\|\mathbf{A}\mathbf{x} - \mathbf{b}\|_2^2$ or $\|\mathbf{A}\mathbf{x} - \mathbf{b}\|_2$ on *real-world* datasets. Simultaneously, we also implement other sparse recovery models, such as L_1 and $L_{1/2}$ [52]. As for L_1 , we solve it by ADMM. In particular, we adopt the following datasets:

- Diabetes dataset ²;
- UCI standard dataset ³: Prostate cancer, Pyrim, Servo, Mpg, Energy and SkillCrift1;
- StatLib datasets archive ⁴: Space-ga.

Each dataset consists of an observation matrix $A \in \mathbb{R}^{m \times n}$ along with the response vector $\mathbf{b} \in \mathbb{R}^{m \times 1}$ and we pre-processing each data (i.e., A and \mathbf{b}) to have mean 0 and squared length 1 in column sense [4].

To evaluate the performance of various algorithms, we divided the dataset randomly into training and test sets with

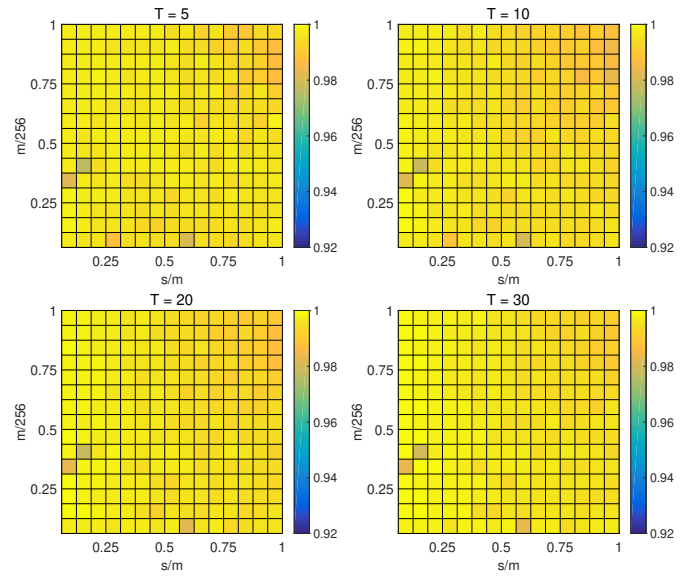


Fig. 4. Each plot depicts the average of $\text{IAcc}(\hat{\mathbf{x}}, \mathbf{x}_T^I)$ across 50 random instances for 256 different problems, where $n = 1024$, $m = 16 : 16 : 256$, and $s = 1 : 1 : 16$. Top row: $T = 5$ (left) and $T = 10$ (right); Bottom row: $T = 20$ (left) and $T = 30$ (right). For $T = 5, 10, 20, 30$, the minimum value of $\text{IAcc}(\hat{\mathbf{x}}, \mathbf{x}_T^I)$ in each plot are 0.98, 0.98, 0.98, 0.98; and the maximum value of $\text{IAcc}(\hat{\mathbf{x}}, \mathbf{x}_T^I)$ in each plot are 1.00, 1.00, 1.00, 1.00.

a specific ratio (*ratio*). After solving the corresponding problem of (1) on the training sets, we evaluate the Mean Squared Error via the test set and define it as

$$\text{TMSE} = \frac{1}{N_{\text{test}}} \|\mathbf{A}_{\text{test}}\mathbf{x} - \mathbf{b}_{\text{test}}\|_2^2,$$

where $\mathbf{A}_{\text{test}}, \mathbf{b}_{\text{test}}$ denote the corresponding observations and response. N_{test} is the number of test data.

For dealing with real data, we replace Line 9 in Algorithm 1 with the following scripts:

- Sort \mathbf{x}^I in ascending order based on absolute values, denoted as \mathbf{x}^\uparrow ;
- Define $\bar{i} \in \arg \max\{i \in [n] \mid \sum_{j=1}^i |x_j^\uparrow| < \tau \|\mathbf{x}^\uparrow\|_1\}$;
- Compute $\hat{\mathbf{x}} = \text{HARD}(\mathbf{x}^I, \mathbf{x}_i^\uparrow)$.

In the initial set of experiments, we conducted tests on the model (1) with $\Phi(\mathbf{x}) = \frac{1}{2}\|\mathbf{A}\mathbf{x} - \mathbf{b}\|_2^2$ by using the ‘Diabetes’ dataset with two different ratios: (a) *ratio*= 8:2 and (b) *ratio*= 7:3. For all algorithms tested, we employed a 10-fold cross-validation on the training set to determine the parameter γ in (1).

For real datasets, the true solutions are *unknown*. Instead of utilizing RErr , we use Relerr (14) to evaluate the performance. Fig. 5 illustrates the variation of Relerr and TMSE with respect to the number of iterations for each algorithm. All these curves represent the average of 100 runs. All algorithms utilized Gaussian random initialization with the `randn` function.

The first row of Fig. 5 displays the TMSE history for each method on the test set under two different ratios (8 : 2 and 7 : 3). It is evident that both ADMM_p and HAFAM_T outperform L_1 and $L_{1/2}$ in terms of TMSE . Furthermore, HAFAM_T rapidly converges to a solution with a smaller TMSE as soon as the semismooth Newton method starts. For HAFAM_T , an

²<https://www4.stat.ncsu.edu/~boos/var.select/diabetes.html>

³<http://archive.ics.uci.edu/datasets>

⁴<http://lib.stat.cmu.edu/datasets/>

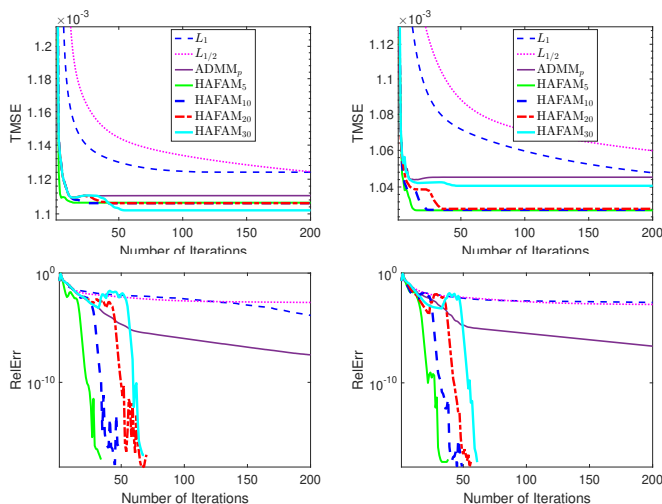


Fig. 5. Comparison among L_1/L_2 via ADMM_p and HAFAM_T , L_1 and $L_{1/2}$. The evolution of test MSE (TMSE) and relative error (RelErr) on diabetes dataset: ratio = 8 : 2 (left); ratio = 7 : 3 (right). ADMM_p and HAFAM_T outperform L_1 and $L_{1/2}$ in terms of TMSE and RelErr. While ADMM_p and HAFAM_T initially overlap in TMSE and RelErr, HAFAM_T quickly converges to a smaller value when the active manifold is identified.

increase in the parameter T increases iterations. This occurs because HAFAM_T needs more iterations to identify the active manifold.

As can be seen, HAFAM_{30} converges to the lowest value of TMSE for the scenario with ratio = 8 : 2. For other values of T (i.e., $T = 5, 10, 20$), HAFAM_T converges to almost the same TMSE under both ratios. However, for the ratio of 7 : 3, HAFAM_{30} converges to a slightly higher TMSE value compared to the other HAFAM_T ($T = 5, 10, 20$), which might be a result of an over-fitting support set.

Regarding RelErr, the curves of ADMM_p and HAFAM_T overlap in the early phases. L_1 and $L_{1/2}$ perform almost the same and much worse than ADMM_p and HAFAM_T . HAFAM_T consistently achieves a smaller RelErr at the termination point compared to the others, and it converges superlinearly after identifying the active manifold.

Next, we conducted numerical simulations for the L_1/L_2 model (1), under two types of data fitting term $\Phi(\mathbf{x}) = \frac{1}{2}\|\mathbf{Ax} - \mathbf{b}\|_2^2$ and $\Phi(\mathbf{x}) = \|\mathbf{Ax} - \mathbf{b}\|_2$ via HAFAM_T (HA_T) and ADMM_p (AD_p) comparing with the corresponding L_1 and $L_{1/2}$ regularization models. The simulations were conducted across various real datasets with a split ratio of 8 : 2. With fine-tuned parameter τ for each scenario, the results are summarized in Tables II-III for $\Phi(\mathbf{x}) = \frac{1}{2}\|\mathbf{Ax} - \mathbf{b}\|_2^2$ and Tables IV-V for $\Phi(\mathbf{x}) = \|\mathbf{Ax} - \mathbf{b}\|_2$, respectively.

The results presented in Tables II,III and IV,V are obtained from an average of 100 independent runs for each instance, and performance is measured in terms of TMSE with standard deviation (std in parentheses), the sparsity of the solution (nnz), and CPU time (CPU) in seconds. The results in these tables correspond to two different initialization strategies: (1) Gaussian random initialization (randn) (Table II and IV) and (2) zero initialization (Table III and V).

As observed from Table II,III and IV,V, HAFAM_T with the L_1/L_2 model is a promising approach, offering improved

accuracy and sparsity compared to traditional L_1 and $L_{1/2}$ regularization. There is minimal difference in TMSE between different initializations for HAFAM_T and ADMM_p , highlighting robustness. Increasing T tends to decrease TMSE and induce sparser solutions. HAFAM_{30} performs the best across most datasets, achieving the lowest TMSE, and HAFAM_T ($T = 5, 10, 20$) shows competitive results.

Interestingly, even with small T , HAFAM_T produces satisfactory results for real datasets. Although increasing T raises TMSE, the impact is not significant, and outcomes depend on specific datasets. Generally, a smaller T in HAFAM_T results in reduced CPU time, while larger T values lead to smaller TMSE. Therefore, it is crucial in practice to carefully select an appropriate value for T in HAFAM_T .

VI. CONCLUSION

We delve into the current popular topic of L_1 over L_2 minimization, verifying its partial smoothness and prox-regularity. Based on this, we validate ADMM_p [10] (or ADMM_p^+ [11]) with the property of identifying the active manifold in finite iterations. *It highlights that these L_1/L_2 proximal-friendly approaches preserve the essential “support detection” property.* It provides a better understanding of the landscape of L_1 over L_2 minimization.

Furthermore, we propose a heuristic acceleration framework. It consists of two phases: first, we employ ADMM_p or ADMM_p^+ to identify the active manifold, then apply a globalized semismooth Newton method within this manifold. Theoretically, we show that it achieves a superlinear/quadratic convergence rate under certain conditions. Extensive numerical experiments for sparse recovery on synthetic and real datasets demonstrate its superiority compared to the existing state-of-the-art methods.

ACKNOWLEDGMENTS

The first author extends gratitude to Prof. Radu Ioan Boț from the University of Vienna for his valuable and constructive comments on the manuscript. The initial version was conducted during she visited him in 2023.

APPENDIX A PROOF OF LEMMA 1

Proof. First, invoking [53, Lemma 2.1(ii)] and $\partial(g(\bar{\mathbf{x}})f(\bar{\mathbf{x}})) = g(\bar{\mathbf{x}})\partial f(\bar{\mathbf{x}})$ (due to f prox-regular at $\bar{\mathbf{x}}$ and $g(\bar{\mathbf{x}}) > 0$),

$$\partial\left(\frac{f}{g}\right)(\bar{\mathbf{x}}) = \frac{g(\bar{\mathbf{x}})\partial f(\bar{\mathbf{x}}) - f(\bar{\mathbf{x}})\nabla g(\bar{\mathbf{x}})}{g(\bar{\mathbf{x}})^2}.$$

We only need to prove for any $\bar{\mathbf{v}} \in \partial f(\bar{\mathbf{x}})$, there exists $\rho > 0$ such that

$$\begin{aligned} \frac{f(\mathbf{y})}{g(\mathbf{y})} - \frac{f(\mathbf{x})}{g(\mathbf{x})} - \left\langle \frac{\mathbf{v}g(\mathbf{x}) - f(\mathbf{x})\nabla g(\mathbf{x})}{g(\mathbf{x})^2}, \mathbf{y} - \mathbf{x} \right\rangle \\ \geq -\frac{\rho}{2}\|\mathbf{x} - \mathbf{y}\|_2^2, \end{aligned} \quad (15)$$

TABLE II

AVERAGE RESULTS ON REAL DATASETS FROM randn INITIALIZATION WITH DATA FIDELITY TERM $\Phi(\cdot) = \|\cdot\|_2^2$. HAFAM_T ACHIEVES MUCH LOWER TMSE AND MUCH SPARSER SOLUTIONS COMPARED WITH OTHERS.

Dataset (m,n)	Algo. (τ)	TMSE (std)	nnz	CPU
Diabetes (422,10)	L_1	1.124e-03 (1.348e-12)	8.00	6.12e+00
	$L_{1/2}$	1.110e-03 (1.430e-07)	9.95	4.84e+00
	AD_p	1.110e-03 (3.672e-11)	8.00	6.44e+00
	HA_5 (0.15)	1.106e-03 (6.971e-14)	7.00	3.36e+01
	HA_{10} (0.10)	1.106e-03 (7.271e-14)	7.00	2.70e+01
	HA_{20} (0.10)	1.106e-03 (1.300e-14)	7.00	3.42e+01
	HA_{30} (0.18)	1.102e-03 (6.192e-14)	6.00	3.28e+01
Prostate cancer (97,8)	L_1	9.542e-01 (5.048e-10)	5.00	5.28e-01
	$L_{1/2}$	8.239e-01 (3.028e-03)	2.02	1.29e-01
	AD_p	7.579e-01 (2.500e-09)	6.00	1.92e+00
	HA_5 (0.15)	7.680e-01 (7.510e-11)	3.00	6.64e+00
	HA_{10} (0.15)	7.680e-01 (4.184e-11)	3.00	5.61e+00
	HA_{20} (0.15)	7.680e-01 (4.149e-11)	3.00	6.53e+00
	HA_{30} (0.15)	7.680e-01 (4.460e-11)	3.00	7.76e+00
Pyrim (74,27)	L_1	2.528e-03 (8.748e-13)	20.00	1.58e+00
	$L_{1/2}$	2.545e-03 (9.937e-05)	18.78	4.45e+00
	AD_p	2.457e-03 (5.152e-13)	22.00	1.17e+01
	HA_5 (0.08)	2.405e-03 (4.192e-05)	15.29	6.31e+00
	HA_{10} (0.08)	2.353e-03 (7.696e-05)	15.99	5.71e+00
	HA_{20} (0.08)	2.310e-03 (9.464e-14)	16.00	9.19e+00
	HA_{30} (0.08)	2.310e-03 (2.638e-13)	16.00	5.82e+00
Servo (167,19)	L_1	6.634e-01 (1.147e-07)	16.00	1.94e+00
	$L_{1/2}$	6.631e-01 (9.635e-05)	17.60	4.63e+00
	AD_p	6.631e-01 (1.303e-07)	16.00	1.10e+01
	HA_5 (0.06)	6.637e-01 (2.027e-02)	13.73	4.72e+01
	HA_{10} (0.08)	6.715e-01 (2.066e-02)	12.93	3.59e+01
	HA_{20} (0.06)	6.621e-01 (1.689e-02)	13.97	3.67e+01
	HA_{30} (0.06)	6.629e-01 (2.003e-02)	13.67	3.88e+01
Mpg (392,7)	L_1	1.003e-03 (2.656e-11)	7.00	6.11e+00
	$L_{1/2}$	1.003e-03 (8.832e-07)	7.00	3.36e+00
	AD_p	1.003e-03 (9.494e-13)	7.00	7.14e-01
	HA_5 (0.10)	9.768e-04 (6.970e-17)	6.00	5.20e-01
	HA_{10} (0.10)	9.768e-04 (3.222e-17)	6.00	6.50e-01
	HA_{20} (0.10)	9.768e-04 (4.535e-17)	6.00	8.85e-01
	HA_{30} (0.10)	9.768e-04 (1.342e-17)	6.00	1.14e+00
Space-ga (3107,6)	L_1	1.436e-04 (4.613e-15)	6.00	8.15e+01
	$L_{1/2}$	1.437e-04 (1.286e-06)	5.41	1.38e+01
	AD_p	1.455e-04 (3.934e-15)	6.00	4.67e+01
	HA_5 (0.05)	1.421e-04 (3.813e-16)	5.00	1.06e+02
	HA_{10} (0.05)	1.421e-04 (1.066e-15)	5.00	1.22e+02
	HA_{20} (0.05)	1.421e-04 (1.369e-14)	5.00	4.94e+02
	HA_{30} (0.05)	1.419e-04 (1.731e-16)	5.00	1.22e+02
Energy (768,8)	L_1	1.156e-04 (2.557e-12)	7.00	1.39e+01
	$L_{1/2}$	1.151e-04 (2.478e-07)	6.91	5.02e+00
	AD_p	1.156e-04 (8.633e-10)	7.00	3.90e+00
	HA_5 (0.10)	1.142e-04 (3.194e-07)	5.13	2.22e+01
	HA_{10} (0.10)	1.142e-04 (3.351e-07)	5.12	1.95e+01
	HA_{20} (0.08)	1.142e-04 (3.352e-07)	5.11	2.87e+01
	HA_{30} (0.08)	1.142e-04 (3.352e-07)	5.11	6.53e+00
SkillCraft1 (3338,18)	L_1	2.294e-04 (2.703e-13)	8.00	2.09e+02
	$L_{1/2}$	2.297e-04 (5.905e-07)	7.09	7.09e+00
	AD_p	2.279e-04 (1.627e-13)	8.00	1.90e+02
	HA_5 (0.02)	2.275e-04 (1.388e-06)	6.83	5.78e+02
	HA_{10} (0.02)	2.271e-04 (8.069e-07)	6.52	5.37e+02
	HA_{20} (0.02)	2.271e-04 (8.087e-07)	6.40	5.48e+02
	HA_{30} (0.02)	2.270e-04 (6.872e-07)	6.20	5.40e+02

TABLE III

AVERAGE RESULTS ON REAL DATASETS FROM ZERO INITIALIZATION WITH DATA FIDELITY TERM $\Phi(\cdot) = \|\cdot\|_2^2$. HAFAM_T OUTPERFORMS THE OTHERS WITH LOWER TMSE AND SPARSER SOLUTIONS. THE FINAL TMSE FROM HAFAM_T IS NOT SENSITIVE TO T .

Dataset (m,n)	Algo. (τ)	TMSE (std)	nnz	CPU
Diabetes (422,10)	L_1	1.110e-03 (2.935e-12)	10.00	2.17e+01
	$L_{1/2}$	1.110e-03 (6.538e-19)	10.00	2.72e+00
	AD_p	1.110e-03 (4.359e-19)	8.00	3.81e+00
	HA_5 (0.10)	1.106e-03 (4.359e-19)	7.00	4.50e-01
	HA_{10} (0.15)	1.106e-03 (6.538e-19)	7.00	5.25e-01
	HA_{20} (0.15)	1.106e-03 (6.538e-19)	7.00	6.80e-01
	HA_{30} (0.10)	1.102e-03 (6.538e-19)	6.00	8.32e-01
Prostate cancer (97,8)	L_1	9.542e-01 (7.811e-16)	5.00	5.65e-01
	$L_{1/2}$	8.423e-01 (1.004e-15)	3.00	1.96e-01
	AD_p	7.579e-01 (8.927e-16)	6.00	2.18e+00
	HA_5 (0.15)	7.680e-01 (1.562e-15)	3.00	3.79e-01
	HA_{10} (0.15)	7.680e-01 (1.116e-15)	3.00	8.81e+01
	HA_{20} (0.15)	7.680e-01 (7.811e-16)	3.00	4.94e-01
	HA_{30} (0.15)	7.680e-01 (6.695e-16)	3.00	6.00e-01
Pyrim (74,27)	L_1	2.516e-03 (1.688e-12)	19.00	3.06e+00
	$L_{1/2}$	2.455e-03 (3.487e-18)	19.00	8.95e+00
	AD_p	2.450e-03 (8.717e-19)	19.00	1.19e+01
	HA_5 (0.08)	2.398e-03 (2.615e-18)	15.00	1.03e+00
	HA_{10} (0.08)	2.309e-03 (1.743e-18)	16.00	2.57e+02
	HA_{20} (0.08)	2.309e-03 (2.179e-18)	16.00	2.33e+00
	HA_{30} (0.08)	2.309e-03 (3.923e-18)	16.00	2.73e+00
Servo (167,19)	L_1	6.634e-01 (1.339e-15)	16.00	3.60e+00
	$L_{1/2}$	6.632e-01 (3.347e-16)	18.00	9.49e+00
	AD_p	6.631e-01 (3.347e-16)	16.00	2.03e+01
	HA_5 (0.08)	6.356e-01 (1.562e-15)	13.00	1.38e+00
	HA_{10} (0.08)	6.356e-01 (7.811e-16)	13.00	1.93e+02
	HA_{20} (0.08)	6.356e-01 (5.579e-16)	13.00	2.05e+02
	HA_{30} (0.08)	6.357e-01 (1.562e-15)	13.00	1.86e+00
Mpg (392,7)	L_1	1.003e-03 (3.339e-12)	7.00	1.18e+01
	$L_{1/2}$	1.003e-03 (1.743e-18)	7.00	6.82e+00
	AD_p	1.003e-03 (1.308e-18)	7.00	1.38e+00
	HA_5 (0.10)	9.768e-04 (1.308e-18)	6.00	9.05e-01
	HA_{10} (0.10)	9.768e-04 (1.308e-18)	6.00	1.11e+00
	HA_{20} (0.10)	9.768e-04 (1.743e-18)	6.00	1.67e+00
	HA_{30} (0.10)	9.768e-04 (2.179e-18)	6.00	2.16e+00
Space-ga (3107,6)	L_1	1.436e-04 (3.814e-19)	6.00	1.37e+02
	$L_{1/2}$	1.430e-04 (2.179e-19)	5.00	2.32e+01
	AD_p	1.455e-04 (1.090e-19)	6.00	7.66e+01
	HA_5 (0.05)	1.421e-04 (8.172e-20)	5.00	5.73e+01
	HA_{10} (0.05)	1.421e-04 (1.634e-19)	5.00	6.47e+01
	HA_{20} (0.05)	1.421e-04 (1.634e-19)	5.00	1.12e+03
	HA_{30} (0.05)	1.419e-04 (0.000e+00)	5.00	9.42e+01
Energy (768,8)	L_1	1.156e-04 (2.179e-19)	7.00	2.03e+01
	$L_{1/2}$	1.149e-04 (1.090e-19)	7.00	9.69e+00
	AD_p	1.156e-04 (1.498e-19)	7.00	7.89e+00
	HA_5 (0.10)	1.141e-04 (5.448e-20)	5.00	3.38e+00
	HA_{10} (0.10)	1.141e-04 (2.724e-20)	5.00	5.76e+00
	HA_{20} (0.08)	1.141e-04 (1.362e-20)	5.00	3.83e+02
	HA_{30} (0.08)	1.141e-04 (1.907e-19)	5.00	9.63e+00
SkillCraft1 (3338,18)	L_1	2.294e-04 (3.269e-19)	8.00	1.96e+02
	$L_{1/2}$	2.299e-04 (5.176e-19)	7.00	6.61e+00
	AD_p	2.279e-04 (1.634e-19)	8.00	1.39e+02
	HA_5 (0.02)	2.269e-04 (2.724e-20)	6.00	8.74e+02
	HA_{10} (0.02)	2.269e-04 (2.452e-19)	6.00	8.70e+01
	HA_{20} (0.02)	2.269e-04 (3.541e-19)	6.00	1.02e+02
	HA_{30} (0.02)	2.269e-04 (2.179e-19)	6.00	1.21e+02

whenever \mathbf{x} and \mathbf{y} are near $\bar{\mathbf{x}}$ with $f(\mathbf{x})/g(\mathbf{x})$ near $f(\bar{\mathbf{x}})/g(\bar{\mathbf{x}})$, and $\frac{\mathbf{v}g(\mathbf{x}) - f(\mathbf{x})\nabla g(\mathbf{x})}{g(\mathbf{x})^2}$ near $\frac{\bar{\mathbf{v}}g(\bar{\mathbf{x}}) - f(\bar{\mathbf{x}})\nabla g(\bar{\mathbf{x}})}{g(\bar{\mathbf{x}})^2}$ (i.e., $\mathbf{v} \in \partial f(\mathbf{x})$ is near $\bar{\mathbf{v}}$). Below, we show that

$$\left| \frac{f(\mathbf{x})}{g(\bar{\mathbf{x}})} - \frac{f(\bar{\mathbf{x}})}{g(\bar{\mathbf{x}})} \right| \leq \left| \frac{f(\mathbf{x})}{g(\bar{\mathbf{x}})} - \frac{f(\mathbf{x})}{g(\mathbf{x})} \right| + \left| \frac{f(\mathbf{x})}{g(\mathbf{x})} - \frac{f(\bar{\mathbf{x}})}{g(\bar{\mathbf{x}})} \right| \\ \leq \frac{|f(\mathbf{x})(g(\mathbf{x}) - g(\bar{\mathbf{x}}))|}{g(\bar{\mathbf{x}})g(\mathbf{x})} + \left| \frac{f(\mathbf{x})}{g(\mathbf{x})} - \frac{f(\bar{\mathbf{x}})}{g(\bar{\mathbf{x}})} \right|.$$

Thus, $f(\mathbf{x})$ near $f(\bar{\mathbf{x}})$ whenever $f(\mathbf{x})/g(\mathbf{x})$ near $f(\bar{\mathbf{x}})/g(\bar{\mathbf{x}})$ and \mathbf{x} near $\bar{\mathbf{x}}$. Since f is prox-regular at the point $\bar{\mathbf{x}}$, then for

the $\bar{\mathbf{v}} \in \partial f(\bar{\mathbf{x}})$, there exists $\rho_1 > 0$ such that

$$f(\mathbf{y}) - f(\mathbf{x}) - \langle \bar{\mathbf{v}}, \mathbf{y} - \mathbf{x} \rangle \geq -\frac{\rho_1}{2} \|\mathbf{x} - \mathbf{y}\|_2^2,$$

whenever \mathbf{x} and \mathbf{y} are near $\bar{\mathbf{x}}$ with $f(\mathbf{x})$ near $f(\bar{\mathbf{x}})$, and $\mathbf{v} \in \partial f(\mathbf{x})$ is near $\bar{\mathbf{v}}$ where $\bar{\mathbf{v}} \in \partial f(\bar{\mathbf{x}})$. In view of $g(\bar{\mathbf{x}}) > 0$, there exists two constants m_1 and M_1 such that

$$0 < m_1 \leq g(\mathbf{x}) \leq M_1, \quad (16)$$

when \mathbf{x} is near $\bar{\mathbf{x}}$. Furthermore,

$$\frac{1}{g(\mathbf{x})} [f(\mathbf{y}) - f(\mathbf{x}) - \langle \bar{\mathbf{v}}, \mathbf{y} - \mathbf{x} \rangle] \geq -\frac{\tilde{\rho}_1}{2} \|\mathbf{x} - \mathbf{y}\|_2^2, \quad (17)$$

TABLE IV

AVERAGE RESULTS ON REAL DATASETS FROM randn INITIALIZATION WITH DATA FIDELITY TERM $\Phi(\cdot) = \|\cdot\|_2$. HAFAM_T CONSISTENTLY OUTPERFORMS OTHERS ACROSS DATASETS.

Datase (m,n)	Algo. (τ)	TMSE (std)	nnz	CPU
Diabetes (422,10)	L_1	1.125e-03 (3.051e-18)	8.00	1.84e+00
	$L_{1/2}$	1.127e-03 (1.481e-05)	7.11	3.22e+00
	AD _p	1.129e-03 (2.396e-05)	7.22	6.59e+00
	HA ₅ (0.15)	1.155e-03 (5.948e-05)	6.50	2.07e+01
	HA ₁₀ (0.15)	1.135e-03 (3.637e-05)	5.99	1.30e+01
	HA ₂₀ (0.15)	1.118e-03 (1.287e-05)	6.08	7.34e+00
	HA ₃₀ (0.15)	1.117e-03 (1.186e-05)	6.06	8.73e+00
Prostate cancer (97,8)	L_1	8.046e-01 (1.674e-15)	7.00	4.56e-01
	$L_{1/2}$	8.078e-01 (4.733e-02)	4.23	1.57e+00
	AD _p	7.659e-01 (2.141e-08)	2.00	2.08e+00
	HA ₅ (0.10)	7.699e-01 (4.687e-03)	3.00	4.44e-01
	HA ₁₀ (0.20)	7.679e-01 (1.617e-11)	3.00	4.87e-01
	HA ₂₀ (0.30)	7.679e-01 (2.032e-11)	3.00	7.54e-01
	HA ₃₀ (0.30)	7.679e-01 (6.917e-11)	3.00	8.67e-01
Pyrim (74,27)	L_1	2.515e-03 (1.743e-18)	19.00	4.83e+00
	$L_{1/2}$	2.698e-03 (2.284e-04)	16.87	4.92e+00
	AD _p	2.465e-03 (2.813e-10)	18.00	8.31e+00
	HA ₅ (0.05)	2.550e-03 (2.543e-04)	14.45	1.31e+01
	HA ₁₀ (0.05)	2.471e-03 (7.683e-05)	15.66	1.61e+01
	HA ₂₀ (0.05)	2.428e-03 (7.465e-06)	15.51	2.15e+01
	HA ₃₀ (0.05)	2.428e-03 (1.156e-06)	15.21	9.97e+00
Servo (167,19)	L_1	6.719e-01 (1.227e-15)	19.00	6.17e+00
	$L_{1/2}$	6.631e-01 (2.535e-04)	18.47	6.69e+00
	AD _p	6.631e-01 (1.139e-05)	17.94	3.07e+01
	HA ₅ (0.01)	6.632e-01 (2.969e-03)	17.51	8.38e+00
	HA ₁₀ (0.01)	6.630e-01 (1.448e-03)	17.42	1.00e+01
	HA ₂₀ (0.01)	6.631e-01 (1.044e-03)	17.48	1.02e+01
	HA ₃₀ (0.01)	6.632e-01 (8.674e-04)	17.39	9.08e+00
Mpg (392,7)	L_1	1.078e-03 (1.308e-18)	4.00	9.52e-01
	$L_{1/2}$	1.038e-03 (1.132e-04)	2.95	3.66e-01
	AD _p	1.022e-03 (8.388e-11)	4.00	1.93e+00
	HA ₅ (0.05)	1.100e-03 (2.227e-04)	3.38	5.60e+01
	HA ₁₀ (0.05)	1.139e-03 (2.817e-04)	3.00	3.73e+01
	HA ₂₀ (0.05)	1.020e-03 (9.156e-07)	3.40	1.14e+00
	HA ₃₀ (0.05)	1.022e-03 (3.663e-07)	3.96	1.47e+00
Space-ga (3107,6)	L_1	1.865e-04 (1.907e-19)	3.00	1.72e+00
	$L_{1/2}$	1.453e-04 (2.997e-07)	6.00	1.88e+01
	AD _p	1.448e-04 (1.619e-13)	6.00	3.71e+01
	HA ₅ (0.01)	1.454e-04 (3.518e-06)	5.73	8.28e-01
	HA ₁₀ (0.01)	1.446e-04 (2.393e-07)	5.63	9.34e-01
	HA ₂₀ (0.01)	1.447e-04 (2.225e-07)	5.72	1.35e+00
	HA ₃₀ (0.01)	1.448e-04 (3.768e-15)	6.00	1.65e+00
Energy (768,8)	L_1	1.277e-04 (1.907e-19)	4.00	6.98e-01
	$L_{1/2}$	1.240e-04 (4.282e-09)	4.00	1.04e+00
	AD _p	1.159e-04 (3.882e-08)	6.83	3.04e+01
	HA ₅ (0.12)	1.210e-04 (1.571e-05)	4.92	3.50e+01
	HA ₁₀ (0.12)	1.200e-04 (3.989e-06)	4.16	1.86e+01
	HA ₂₀ (0.12)	1.179e-04 (3.818e-06)	4.00	1.29e+00
	HA ₃₀ (0.12)	1.155e-04 (8.291e-07)	4.00	1.56e+00
SkillCraft1 (3338,18)	L_1	2.293e-04 (2.724e-20)	8.00	2.74e+00
	$L_{1/2}$	2.297e-04 (5.408e-07)	7.19	3.55e+00
	AD _p	2.278e-04 (4.941e-13)	8.00	5.74e+00
	HA ₅ (0.05)	2.338e-04 (2.319e-05)	8.64	4.82e+00
	HA ₁₀ (0.05)	2.283e-04 (2.883e-06)	7.21	2.51e+00
	HA ₂₀ (0.05)	2.283e-04 (2.487e-06)	6.65	3.16e+00
	HA ₃₀ (0.05)	2.275e-04 (1.230e-06)	6.43	3.54e+00

TABLE V

AVERAGE RESULTS ON REAL DATASETS FROM ZERO INITIALIZATION WITH DATA FIDELITY TERM $\Phi(\cdot) = \|\cdot\|_2$. HAFAM_T CONTINUES TO PERFORM WELL.

Datase (m,n)	Algo. (τ)	TMSE (std)	nnz	CPU
Diabetes (422,10)	L_1	1.125e-03 (3.051e-18)	8.00	1.72e+00
	$L_{1/2}$	1.129e-03 (1.526e-18)	7.00	1.05e+00
	AD _p	1.125e-03 (1.526e-18)	7.00	3.35e+00
	HA ₅ (0.15)	1.122e-03 (1.526e-18)	6.00	4.51e-01
	HA ₁₀ (0.15)	1.132e-03 (1.526e-18)	6.00	5.17e-01
	HA ₂₀ (0.15)	1.122e-03 (8.717e-19)	6.00	1.32e+00
	HA ₃₀ (0.15)	1.122e-03 (2.833e-18)	6.00	2.49e+00
Prostate cancer (97,8)	L_1	8.046e-01 (1.674e-15)	7.00	4.20e-01
	$L_{1/2}$	8.407e-01 (3.347e-16)	5.00	1.35e+00
	AD _p	7.659e-01 (0.000e+00)	2.00	2.13e+00
	HA ₅ (0.10)	7.679e-01 (6.695e-16)	3.00	4.45e-01
	HA ₁₀ (0.20)	7.679e-01 (1.227e-15)	3.00	4.94e-01
	HA ₂₀ (0.30)	7.679e-01 (1.562e-15)	3.00	7.82e-01
	HA ₃₀ (0.30)	7.679e-01 (1.116e-16)	3.00	8.80e-01
Pyrim (74,27)	L_1	2.520e-03 (3.487e-18)	21.00	3.43e+00
	$L_{1/2}$	2.550e-03 (2.179e-18)	17.00	4.96e+00
	AD _p	2.465e-03 (4.359e-18)	18.00	8.01e+00
	HA ₅ (0.05)	2.870e-03 (7.410e-18)	13.00	1.99e+00
	HA ₁₀ (0.05)	2.429e-03 (1.743e-18)	15.00	1.40e+00
	HA ₂₀ (0.05)	2.429e-03 (1.308e-18)	15.00	1.52e+00
	HA ₃₀ (0.05)	2.429e-03 (6.538e-18)	15.00	1.59e+00
Servo (167,19)	L_1	6.653e-01 (1.562e-15)	19.00	6.40e+00
	$L_{1/2}$	6.630e-01 (1.116e-15)	18.00	6.79e+00
	AD _p	6.633e-01 (1.116e-16)	18.00	3.09e+01
	HA ₅ (0.05)	6.622e-01 (3.347e-16)	15.00	8.34e+00
	HA ₁₀ (0.05)	6.736e-01 (3.347e-16)	13.00	8.41e-01
	HA ₂₀ (0.08)	6.640e-01 (4.463e-16)	13.00	9.45e-01
	HA ₃₀ (0.08)	6.529e-01 (2.232e-16)	13.00	9.42e+00
Mpg (392,7)	L_1	1.078e-03 (1.308e-18)	4.00	8.90e-01
	$L_{1/2}$	1.057e-03 (1.743e-18)	3.00	3.37e-01
	AD _p	1.022e-03 (1.090e-18)	4.00	1.91e+00
	HA ₅ (0.05)	1.082e-03 (1.743e-18)	2.00	2.92e-01
	HA ₁₀ (0.05)	1.020e-03 (4.359e-19)	3.00	2.11e+01
	HA ₂₀ (0.05)	1.020e-03 (1.090e-18)	3.00	7.16e-01
	HA ₃₀ (0.05)	1.022e-03 (2.397e-18)	4.00	1.11e+00
Space-ga (3107,6)	L_1	1.865e-04 (1.907e-19)	3.00	1.65e+00
	$L_{1/2}$	1.454e-04 (2.179e-19)	6.00	1.94e+01
	AD _p	1.448e-04 (2.179e-19)	6.00	3.95e+01
	HA ₅ (0.01)	1.640e-04 (2.724e-19)	5.00	9.69e-01
	HA ₁₀ (0.01)	1.443e-04 (2.997e-19)	5.00	9.67e-01
	HA ₂₀ (0.01)	1.448e-04 (2.997e-19)	6.00	1.98e+00
	HA ₃₀ (0.01)	1.448e-04 (8.172e-20)	6.00	1.83e+00
Energy (768,8)	L_1	1.277e-04 (1.907e-19)	4.00	6.87e-01
	$L_{1/2}$	1.240e-04 (1.907e-19)	4.00	1.39e+00
	AD _p	1.158e-04 (1.090e-19)	6.00	2.82e+01
	HA ₅ (0.12)	1.166e-04 (1.090e-19)	4.00	6.77e-01
	HA ₁₀ (0.12)	1.166e-04 (1.090e-19)	4.00	7.18e-01
	HA ₂₀ (0.12)	1.154e-04 (1.907e-19)	4.00	8.46e-01
	HA ₃₀ (0.12)	1.154e-04 (9.535e-20)	4.00	1.84e+00
SkillCraft1 (3338,18)	L_1	2.293e-04 (2.724e-20)	8.00	2.42e+00
	$L_{1/2}$	2.296e-04 (4.903e-19)	8.00	2.53e+00
	AD _p	2.278e-04 (2.452e-19)	8.00	3.61e+00
	HA ₅ (0.05)	2.276e-04 (1.907e-19)	6.00	8.35e-01
	HA ₁₀ (0.05)	2.278e-04 (4.359e-19)	6.00	9.77e-01
	HA ₂₀ (0.05)	2.278e-04 (4.359e-19)	6.00	1.15e+00
	HA ₃₀ (0.05)	2.276e-04 (1.634e-19)	6.00	1.41e+00

where $\tilde{\rho}_1 = \rho_1/m_1$. To proceed, we verify the following inequality:

$$\begin{aligned} & \frac{f(\mathbf{y})}{g(\mathbf{y})} \frac{1}{g(\mathbf{x})} (g(\mathbf{x}) - g(\mathbf{y})) + \frac{f(\mathbf{x})}{g(\mathbf{x})^2} \langle \nabla g(\mathbf{x}), \mathbf{y} - \mathbf{x} \rangle \\ & \geq -\frac{\rho_2}{2} \|\mathbf{x} - \mathbf{y}\|_2^2. \end{aligned} \quad (18)$$

We divide into two cases to prove: (a) $f(\mathbf{x}) = 0$; (b) $f(\mathbf{x}) \neq 0$. Case (a): $f(\mathbf{x}) = 0$. If $f(\mathbf{y}) = 0$, the above inequality holds obviously. If $f(\mathbf{y}) \neq 0$, Because f is locally Lipschitz continuous $\bar{\mathbf{x}}$, there exist two constants m_2 and M_2 such that $m_2 \leq f(\mathbf{y}) \leq M_2$ (M_2, m_2 can take the same sign as $f(\mathbf{y})$) when \mathbf{y} is near $\bar{\mathbf{x}}$. Without loss of generality, we assume that $m_2 > 0$. By using the locally Lipschitz continuity of g near

$\bar{\mathbf{x}}$ (with constant L_g) and combining with (16), there exists a constant ρ_2 such that (18) holds.

Case (b): $f(\mathbf{x}) \neq 0$. We first show that $H(\mathbf{x}) = \frac{f(\mathbf{x})}{g(\mathbf{x})}$ is locally Lipschitz continuous around $\bar{\mathbf{x}}$. Let $L_H = \frac{M_2}{m_1^2} L_g + \frac{L_f}{m_1}$.

$$\begin{aligned} |H(\mathbf{x}) - H(\mathbf{y})| & \leq \frac{H(\mathbf{x})}{g(\mathbf{y})} |g(\mathbf{y}) - g(\mathbf{x})| + \frac{1}{g(\mathbf{y})} |f(\mathbf{x}) - f(\mathbf{y})| \\ & \leq L_H \|\mathbf{x} - \mathbf{y}\|_2. \end{aligned}$$

$$\begin{aligned}
& \frac{f(\mathbf{y})}{g(\mathbf{y})g(\mathbf{x})} (g(\mathbf{x}) - g(\mathbf{y})) + \frac{f(\mathbf{x})}{g(\mathbf{x})^2} \langle \nabla g(\mathbf{x}), \mathbf{y} - \mathbf{x} \rangle \\
&= \frac{1}{g(\mathbf{x})} (H(\mathbf{y}) - H(\mathbf{x})) (g(\mathbf{x}) - g(\mathbf{y})) \\
&+ \frac{f(\mathbf{x})}{g(\mathbf{x})^2} (g(\mathbf{x}) - g(\mathbf{y})) + \langle \nabla g(\mathbf{x}), \mathbf{y} - \mathbf{x} \rangle \\
&\geq -\frac{1}{m_1} L_H L_g \|\mathbf{x} - \mathbf{y}\|_2^2 - \frac{L_{\nabla g} M_2}{2 m_1^2} \|\mathbf{x} - \mathbf{y}\|_2^2,
\end{aligned}$$

where $L_{\nabla g}$ is the locally Lipschitz constants of ∇g . Thus, the inequality (18) is valid with $\rho_2 = \frac{2L_H L_g}{m_1} + \frac{M_2 L_{\nabla g}}{m_1^2}$.

By multiplying (17) on both sides with $\frac{g(\mathbf{y})}{g(\mathbf{x})}$ and adding with (18), it leads to (15) is valid with $\rho = \tilde{\rho}_1 + \rho_2$. Therefore, the function $\frac{f}{g}$ is prox-regular at the point $\bar{\mathbf{x}}$. \square

APPENDIX B

PROOF OF PROPOSITION 1

Proof. First, we show that $h(\cdot)$ defined in (4) is partly smooth at \mathbf{x}_0 relative to $\mathcal{M}_{\mathbf{x}_0}$. We divide into two cases to verify: (a) $\mathcal{X} = \mathbb{R}^n$; (b) $\mathcal{X} = \mathbb{R}_+^n$.

Case (a). By invoking Definition 2, it is evident that properties (i) and (iv) hold. Additionally, we can refer to Equation (2.3) in [13] to show the validity of property (ii). We only need to verify the property (iii) normal sharpness, i.e.,

$$dh(\mathbf{x}_0)(-\mathbf{w}) > -dh(\mathbf{x}_0)(\mathbf{w})$$

for all nonzero directions \mathbf{w} in $N_{\mathcal{M}_{\mathbf{x}_0}}(\mathbf{x})$. Note that

$$h(\mathbf{x}_0 + \tau\mathbf{w}) = \frac{\|\mathbf{x}_0 + \tau\mathbf{w}\|_1}{\|\mathbf{x}_0 + \tau\mathbf{w}\|_2} = \frac{\|\mathbf{x}_0\|_1 + \tau\|\mathbf{w}\|_1}{\sqrt{\|\mathbf{x}_0\|_2^2 + \tau^2\|\mathbf{w}\|_2^2}}$$

when \mathbf{w} in $N_{\mathcal{M}_{\mathbf{x}_0}}(\mathbf{x})$. Recall $h(\cdot)$ is defined in (4). By some routine calculations, it yields that

$$dh(\mathbf{x}_0)(\mathbf{w}) = \lim_{\tau \downarrow 0} \inf_{\bar{\mathbf{w}} \rightarrow \mathbf{w}} \frac{h(\mathbf{x}_0 + \tau\bar{\mathbf{w}}) - h(\mathbf{x}_0)}{\tau} = \frac{\|\mathbf{w}\|_1}{\|\mathbf{x}_0\|_2},$$

and

$$dh(\mathbf{x}_0)(-\mathbf{w}) = \lim_{\tau \downarrow 0} \inf_{\bar{\mathbf{w}} \rightarrow \mathbf{w}} \frac{h(\mathbf{x}_0 - \tau\bar{\mathbf{w}}) - h(\mathbf{x}_0)}{\tau} = \frac{\|\mathbf{w}\|_1}{\|\mathbf{x}_0\|_2}.$$

Thus, the property (iii) of Definition 2 holds for the $h(\cdot)$ defined in (4).

Case (b). The proof for property (i)-(iii) are similar to Case (a). For (iv), we only need to show that ∂h is inner semicontinuous at \mathbf{x}_0 relative $\mathcal{M}_{\mathbf{x}_0}$. First note that

$$h(\mathbf{x}) = h_1(\mathbf{x}) + \iota_{\mathbb{R}_+^n}(\mathbf{x}),$$

where $h_1(\mathbf{x}) := \frac{\mathbf{e}^\top \mathbf{x}}{\|\mathbf{x}\|_2}$. According to [42, Corollary 10.9 and Exercise 10.10], we have

$$\partial h(\mathbf{x}) = \partial h_1(\mathbf{x}) + N_{\mathbb{R}_+^n}(\mathbf{x}), \quad (19)$$

where $N_{\mathbb{R}_+^n}(\mathbf{x})$ is the limiting normal cone of \mathbb{R}_+^n at \mathbf{x} .

$$N_{\mathbb{R}_+^n}(\mathbf{x}) = \{\mathbf{d} \in \mathbb{R}^n \mid \mathbf{d}_\Lambda = \mathbf{0}, \mathbf{d}_{\Lambda^c} \leq \mathbf{0}, \Lambda = \text{supp}(\mathbf{x})\}, \quad (20)$$

and invoking [53, Lemma 2.1(ii)], $\partial h_1(\mathbf{x}) = \frac{\mathbf{e}}{r} - \frac{a}{r^3} \mathbf{x}$, where $a = \|\mathbf{x}\|_1$ and $r = \|\mathbf{x}\|_2$.

Next, without loss of generality, we assume that $(\mathbf{x}_0)^\top = ((\mathbf{x}_1)^\top, (\mathbf{x}_2)^\top)$ where $\mathbf{x}_1 = (\mathbf{x}_0)_\Lambda$ ($\Lambda = \text{supp}(\mathbf{x}_0)$) and $\mathbf{x}_2 = \mathbf{0}$.

For any $\mathbf{y} \in \partial h(\mathbf{x}_0)$, it follows from (19) and (20) that

$$\mathbf{y} = \left(\frac{\mathbf{e}}{r} - \frac{a}{r^3} \mathbf{x}_0 \right) + \mathbf{d} \quad (21)$$

where $a = \|\mathbf{x}_0\|_1$ and $r = \|\mathbf{x}_0\|_2$ and $(\mathbf{d})^\top = ((\mathbf{d}_1)^\top, (\mathbf{d}_2)^\top)$ (where \mathbf{d}_1 and \mathbf{d}_2 are in the same dimension as \mathbf{x}_1 and \mathbf{x}_2) and $\mathbf{d}_1 = \mathbf{0} \in \mathbb{R}^{\#(\Lambda)}$ and $\mathbf{d}_2 \leq \mathbf{0}$.

For any sequence of points \mathbf{x}^k in $\mathcal{M}_{\mathbf{x}_0}$ approaching \mathbf{x}_0 , we take $\mathbf{y}^k = \left(\frac{\mathbf{e}}{r_k} - \frac{a_k}{(r_k)^3} \mathbf{x}^k \right) + \mathbf{d}$ ($a_k = \|\mathbf{x}^k\|_1$, $r_k = \|\mathbf{x}^k\|_2$) where \mathbf{d} is given in (21). We have $\mathbf{y}^k \in \partial h(\mathbf{x}^k)$ due to $\mathbf{x}^k \in \mathcal{M}_{\mathbf{x}_0}$ and $\mathbf{y}^k \rightarrow \mathbf{y}$. Thus, ∂h is inner semicontinuous at \mathbf{x}_0 relative $\mathcal{M}_{\mathbf{x}_0}$. So, h is partly smooth at any \mathbf{x}_0 relative to $\mathcal{M}_{\mathbf{x}_0}$.

For both cases, we show that $h(\cdot)$ defined in (4) is partly smooth at \mathbf{x}_0 relative to $\mathcal{M}_{\mathbf{x}_0}$. Invoking [39, Corollary 4.7], $F_u(\cdot) + \iota_{\mathcal{X}}(\cdot)$ is partly smooth at \mathbf{x}_0 relative to $\mathcal{M}_{\mathbf{x}_0}$. \square

APPENDIX C

PROOF OF THEOREM 4

Proof. First, we have $\mathbf{x}^\infty \neq \mathbf{0}$ due to $A^\top \mathbf{b} \notin \mathcal{X}^o$. For the comprehensive proof of this argument, we refer the reader to the detailed proof of [10, Theorem 5.8] and [11, Theorem 8]. For the model (1) with the general $\Phi(\mathbf{x})$ (L -smooth), the global convergence of (5) holds according to Theorem 2. For either $\mathcal{X} = \mathbb{R}_+^n$ or $\mathcal{X} = \mathbb{R}^n$, according to [42, Corollary 10.9], the following relation holds

$$\partial \left(\frac{\|\cdot\|_1}{\|\cdot\|_2} + \iota_{\mathcal{X}}(\cdot) \right) (\mathbf{x}) = \partial \frac{\|\mathbf{x}\|_1}{\|\mathbf{x}\|_2} + \partial \iota_{\mathcal{X}}(\mathbf{x}). \quad (22)$$

This is a consequence of the regularity of both $\frac{\|\cdot\|_1}{\|\cdot\|_2}$ and $\iota_{\mathcal{X}}(\cdot)$. By invoking the optimality condition of (5) and combining (22), we have that

$$\begin{cases}
\mathbf{0} \in \gamma \left(\frac{\text{sign}(\mathbf{x}^{k+1})}{r_{k+1}} - \frac{a_{k+1}}{(r_{k+1})^3} \mathbf{x}^{k+1} + \partial \iota_{\mathcal{X}}(\mathbf{x}^{k+1}) \right) \\
+ \beta \left(\mathbf{x}^{k+1} - \mathbf{y}^k + \frac{\mathbf{z}^k}{\beta} \right) \\
\nabla \Phi(\mathbf{y}^{k+1}) + \beta(\mathbf{y}^{k+1} - \mathbf{x}^{k+1} - \frac{1}{\beta} \mathbf{z}^k) = \mathbf{0} \\
\mathbf{z}^{k+1} = \mathbf{z}^k + \beta(\mathbf{x}^{k+1} - \mathbf{y}^{k+1}),
\end{cases}$$

where $a_{k+1} = \|\mathbf{x}^{k+1}\|_1$ and $r_{k+1} = \|\mathbf{x}^{k+1}\|_2$. By substituting the third into the second, we have $\nabla \Phi(\mathbf{y}^{k+1}) = \mathbf{z}^{k+1}$. Furthermore, by invoking (22), we arrive at

$$\begin{aligned}
& \text{dist}(\partial(F_u(\cdot) + \iota_{\mathcal{X}}(\cdot))(\mathbf{x}^{k+1}), \mathbf{0}) \\
&= \text{dist} \left[\gamma \left(\frac{\text{sign}(\mathbf{x}^{k+1})}{r_{k+1}} - \frac{a_{k+1}}{(r_{k+1})^3} \mathbf{x}^{k+1} + \partial \iota_{\mathcal{X}}(\mathbf{x}^{k+1}) \right) \right. \\
&\quad \left. + \nabla \Phi(\mathbf{x}^{k+1}), \mathbf{0} \right] \\
&\leq \left\| -\beta(\mathbf{x}^{k+1} - \mathbf{y}^k + \frac{1}{\beta} \mathbf{z}^k) + \nabla \Phi(\mathbf{x}^{k+1}) \right\|_2 \\
&= \left\| -\mathbf{z}^{k+1} + \beta(\mathbf{y}^k - \mathbf{y}^{k+1}) + \nabla \Phi(\mathbf{x}^{k+1}) \right\|_2 \\
&= \left\| -\nabla \Phi(\mathbf{y}^{k+1}) + \nabla \Phi(\mathbf{x}^{k+1}) + \beta(\mathbf{y}^k - \mathbf{y}^{k+1}) \right\|_2 \\
&\leq L \|\mathbf{x}^{k+1} - \mathbf{y}^{k+1}\|_2 + \beta \|\mathbf{y}^k - \mathbf{y}^{k+1}\|_2 \\
&\leq \frac{L}{\beta} \|\mathbf{z}^k - \mathbf{z}^{k+1}\|_2 + \beta \|\mathbf{y}^k - \mathbf{y}^{k+1}\|_2.
\end{aligned}$$

On the other hand, it follows from $\nabla\Phi(\mathbf{y}^{k+1}) = \mathbf{z}^{k+1}$ that

$$\|\mathbf{z}^{k+1} - \mathbf{z}^k\|_2 = \|\nabla\Phi(\mathbf{y}^{k+1}) - \nabla\Phi(\mathbf{y}^k)\|_2 \leq L\|\mathbf{y}^{k+1} - \mathbf{y}^k\|_2.$$

By combining the last two inequalities, we have

$$\begin{aligned} & \text{dist}(\partial(F_u(\cdot) + \iota_{\mathcal{X}}(\cdot))(\mathbf{x}^{k+1}), \mathbf{0}) \\ & \leq \left(\frac{L^2}{\beta} + \beta\right) \|\mathbf{y}^k - \mathbf{y}^{k+1}\|_2 \rightarrow 0, \end{aligned}$$

as $k \rightarrow \infty$.

In addition, the function $F_u(\mathbf{x}) + \iota_{\mathcal{X}}(\mathbf{x})$ is partly smooth at the point \mathbf{x}^∞ relative to the manifold $\mathcal{M}_{\mathbf{x}^\infty}$ (as shown in Proposition 1). Next, we show it is prox-regular at \mathbf{x}^∞ . From Definition 1, we see that $f(\cdot) = \|\cdot\|_1 + \iota_{\mathcal{X}}(\cdot)$ is prox-regular \mathbf{x}^∞ for $\mathcal{X} = \mathbb{R}^n$ or $\mathcal{X} = \mathbb{R}_+^n$. Thus, by setting $f(\cdot) = \|\cdot\|_1 + \iota_{\mathcal{X}}(\cdot)$ and $g(\cdot) = \|\cdot\|_2$ in Lemma 1, we have that $h(\cdot)$ defined in (4) is prox-regular at \mathbf{x}^∞ .

Invoking [53, Lemma 2.1(i)], we have that

$$\partial(h + \Phi)(\mathbf{x}) = \partial h(\mathbf{x}) + \nabla\Phi(\mathbf{x}),$$

due to h and Φ are regular. Noting that for any $\mathbf{v} \in \partial(F_u + \iota_{\mathcal{X}})(\mathbf{x}^\infty)$, we have $\mathbf{v} = \mathbf{v}_1 + \mathbf{v}_2$ where $\mathbf{v}_1 \in \partial h(\mathbf{x}^\infty)$ and $\mathbf{v}_2 \in \nabla\Phi(\mathbf{x}^\infty)$. By using $h(\cdot)$ and $\Phi(\cdot)$ are prox-regular at \mathbf{x}^∞ and recall Definition 1, we can obtain that $F_u(\cdot) + \iota_{\mathcal{X}}(\cdot)$ is prox-regular at \mathbf{x}^∞ . According to Theorem 3, we have that for all large k , $\mathbf{x}_k \in \mathcal{M}_{\mathbf{x}^\infty}$. \square

APPENDIX D PROOF OF THEOREM 5

Proof. The assertion (i) is valid obviously. For (ii), the direction \mathbf{u}^j is always a decent direction of $\varphi(\cdot)$ if the sequence doesn't achieve the stationary point (i.e., $\varphi(\hat{\mathbf{u}}) = 0$). Since φ is level bounded on $\mathcal{M}_{\mathbf{x}^\infty}$, the sequence of $\{\mathbf{u}^j\}$ is bounded. Assume that $\hat{\mathbf{u}}$ be an accumulation point of $\{\mathbf{u}^j\}$. Then, there exists a subsequence $\{\mathbf{u}^{k_j}\}$ converging to $\hat{\mathbf{u}}$ and $\nabla\varphi(\hat{\mathbf{u}}) = 0$ by using the standard analysis [54, Theorem 6.3.3].

Next, invoking for all $V \in \partial^2\varphi(\hat{\mathbf{u}})$ positive definite, then there exists an open ball $\mathcal{B}(\hat{\mathbf{u}})$ centered at $\hat{\mathbf{u}}$ such that the matrices set of $\mathcal{V} = \{V \in \partial^2\varphi(\mathbf{u}) | \mathbf{u} \in \mathcal{B}(\hat{\mathbf{u}})\}$ are uniformly positive definite. Next, we show that for j sufficiently large, $V_{k_j} \in \mathcal{V}$, we can always find an approximate solution of \mathbf{d}^{k_j} of (12) with $j := k_j$ such that both (13) with $j := k_j$ and

$$\langle \nabla\varphi(\mathbf{u}^{k_j}), \mathbf{d}^{k_j} \rangle \leq -\nu_{k_j} \|\mathbf{d}^{k_j}\|_2^2 \quad (23)$$

hold. Additionally, (13) with $j := k_j$ leads to

$$\|\nabla\varphi(\mathbf{u}^{k_j})\|_2 \leq \frac{1}{1-\eta} \|V_{k_j}\|_2 \|\mathbf{d}^{k_j}\|_2. \quad (24)$$

Below, we prove in two steps: (a) there exists a subsequence $\{\mathbf{d}^{k_j}\}$ such that (12), (13) and (23) hold. (b) Using induction, we can see that there exists an index \hat{k} such that for $j \geq \hat{k}$, $\mathbf{u}^j \in \mathcal{B}(\hat{\mathbf{u}})$, $\alpha_j = 1$ (taking unit step size).

(a) Since the set \mathcal{V} is uniformly positive definite, and define $\rho = \inf_{V \in \mathcal{V}} \lambda_{\min}(V)$ and thus $\rho > 0$. There exists

a subsequence k_j such that $\nabla\varphi(\mathbf{u}^{k_j}) \rightarrow 0$ and an approximate solution $\hat{\mathbf{d}}^{k_j}$ of (12) satisfying

$$\begin{aligned} & \langle \nabla\varphi(\mathbf{u}^{k_j}), \hat{\mathbf{d}}^{k_j} \rangle \\ & = \langle \nabla\varphi(\mathbf{u}^{k_j}) + V_{k_j} \hat{\mathbf{d}}^{k_j}, \hat{\mathbf{d}}^{k_j} \rangle - \langle V_{k_j} \hat{\mathbf{d}}^{k_j}, \hat{\mathbf{d}}^{k_j} \rangle \\ & \stackrel{(13)}{\leq} \eta_{k_j} \|\nabla\varphi(\mathbf{u}^{k_j})\|_2 \|\hat{\mathbf{d}}^{k_j}\|_2 - \rho \|\hat{\mathbf{d}}^{k_j}\|_2^2 \\ & \leq \|\nabla\varphi(\mathbf{u}^{k_j})\|_2^2 \|\hat{\mathbf{d}}^{k_j}\|_2 - \rho \|\hat{\mathbf{d}}^{k_j}\|_2^2 \\ & \leq \frac{1}{1-\eta} \|V_{k_j}\|_2 \|\hat{\mathbf{d}}^{k_j}\|_2^2 \|\nabla\varphi(\mathbf{u}^{k_j})\|_2 - \rho \|\hat{\mathbf{d}}^{k_j}\|_2^2 \\ & \leq -\frac{\rho}{2} \|\hat{\mathbf{d}}^{k_j}\|_2^2, \end{aligned} \quad (25)$$

The third-to-last and the last inequalities of (25) are due to the definition of η_{k_j} and $\nabla\varphi(\mathbf{u}^{k_j}) \rightarrow 0$, respectively. The penultimate is due to (24). Inequality (25) implies that $\hat{\mathbf{d}}^{k_j}$ satisfies (12), (13) and (23). It follows from [49, Lemma 5.2] that for all sufficiently large j , $\alpha_{k_j} = 1$, and $\mathbf{u}^{k_j+1} = \mathbf{u}^{k_j} + \mathbf{d}^{k_j}$.

(b) By invoking $\nabla\varphi$ is semismooth at $\hat{\mathbf{u}}$ or $\nabla\varphi$ is strongly semismooth at $\hat{\mathbf{u}}$, for sufficiently large k , we have

$$\|\mathbf{u}^k + \mathbf{d}^k - \hat{\mathbf{u}}\|_2 = o(\|\mathbf{u}^k - \hat{\mathbf{u}}\|_2)$$

or

$$\|\mathbf{u}^k + \mathbf{d}^k - \hat{\mathbf{u}}\|_2 = O(\|\mathbf{u}^k - \hat{\mathbf{u}}\|_2^2),$$

respectively. Then, for all sufficiently large j , $\mathbf{u}^{k_j} \in \mathcal{B}(\hat{\mathbf{u}})$, thus $\mathbf{u}^{k_j+1} \in \mathcal{B}(\hat{\mathbf{u}})$. Then, following the above proof, we see that $V_{k_j+1} \in \mathcal{V}$ and there exists \mathbf{d}^{k_j+1} satisfying (12), (13) and (23). Thus, $\alpha_{k_j+1} = 1$. By induction, there exists an index k_J such that for $j \geq k_J$, $\mathbf{u}^j \in \mathcal{B}(\hat{\mathbf{u}})$, $\alpha_j = 1$ (taking unit step size).

The assertion (ii) follows directly. Clearly, assertion (iii) is valid. \square

REFERENCES

- [1] R. G. Baraniuk, E. Candes, M. Elad, and Y. Ma, "Applications of sparse representation and compressive sensing," *Proc. IEEE*, vol. 98, no. 6, pp. 906–909, 2010.
- [2] Z. Wen, W. Yin, D. Goldfarb, and Y. Zhang, "A fast algorithm for sparse reconstruction based on shrinkage, subspace optimization, and continuation," *SIAM J. Sci. Comput.*, vol. 32, no. 4, pp. 1832–1857, 2010.
- [3] J. Shi, W. Yin, S. Osher, and P. Sajda, "A fast hybrid algorithm for large-scale ℓ_1 -regularized logistic regression," *J. Mach. Learn. Res.*, vol. 11, pp. 713–741, 2010.
- [4] T. Hastie, R. Tibshirani, J. H. Friedman, and J. H. Friedman, *The elements of statistical learning: data mining, inference, and prediction*. Springer, 2009.
- [5] D. Krishnan, T. Tay, and R. Fergus, "Blind deconvolution using a normalized sparsity measure," in *CVPR*, 2011, pp. 233–240.
- [6] A. Repetti, M. Q. Pham, L. Duval, E. Chouzenoux, and J.-C. Pesquet, "Euclid in a taxicab: Sparse blind deconvolution with smoothed ℓ_1/ℓ_2 regularization," *IEEE Signal Process Lett.*, vol. 22, no. 5, pp. 539–543, 2015.
- [7] X. Fu, K. Huang, N. D. Sidiropoulos, and W.-K. Ma, "Nonnegative matrix factorization for signal and data

- analytics: Identifiability, algorithms, and applications,” *IEEE Signal Proc. Mag.*, vol. 36, no. 2, pp. 59–80, 2019.
- [8] E. Esser, Y. Lou, and J. Xin, “A method for finding structured sparse solutions to nonnegative least squares problems with applications,” *SIAM J. Imaging Sci.*, vol. 6, no. 4, pp. 2010–2046, 2013.
- [9] P. Yin, E. Esser, and J. Xin, “Ratio and difference of ℓ_1 and ℓ_2 norms and sparse representation with coherent dictionaries,” *Comm. Info. Systems*, vol. 14, no. 2, pp. 87–109, 2014.
- [10] M. Tao, “Minimization of L_1 over L_2 for sparse signal recovery with convergence guarantee,” *SIAM J. Sci. Comput.*, vol. 44, no. 2, pp. A770–A797, 2022.
- [11] M. Tao and X.-P. Zhang, “Study on L_1 over L_2 minimization for nonnegative signal recovery,” *J. Sci. Comp.*, vol. 95, 2023.
- [12] Y. Xu, A. Narayan, H. Tran, and C. G. Webster, “Analysis of the ratio of ℓ_1 and ℓ_2 norms in compressed sensing,” *Appl. Comput. Harmon. Anal.*, vol. 55, pp. 486–511, 2021.
- [13] L. Y. Zeng, P. R. Yu, and T. K. Pong, “Analysis and algorithms for some compressed sensing models based on L_1/L_2 minimization,” *SIAM J. Optim.*, vol. 31, no. 2, pp. 1576–1603, 2021.
- [14] Y. Rahimi, C. Wang, H. Dong, and Y. Lou, “A scale-invariant approach for sparse signal recovery,” *SIAM J. Sci. Comput.*, vol. 41, no. 6, pp. A3649–A3672, 2019.
- [15] M. Q. Pham, B. Oudompheng, J. I. Mars, and B. Nicolas, “A noise-robust method with smoothed ℓ_1/ℓ_2 regularization for sparse moving-source mapping,” *Signal Process.*, vol. 135, pp. 96–106, 2017.
- [16] N. Hurley and S. Rickard, “Comparing measures of sparsity,” *IEEE Trans. Inf. Theory*, vol. 55, no. 10, pp. 4723–4741, 2009.
- [17] D. L. Donoho and M. Elad, “Optimally sparse representation in general (nonorthogonal) dictionaries via ℓ^1 minimization,” *PNAS*, vol. 100, no. 5, pp. 2197–2202, 2003.
- [18] R. Gribonval and M. Nielsen, “Sparse representations in unions of bases,” *IEEE Trans. Inform. Theory*, vol. 49, no. 12, pp. 3320–3325, 2003.
- [19] A. Benichoux, E. Vincent, and R. Gribonval, “A fundamental pitfall in blind deconvolution with sparse and shift-invariant priors,” in *ICASSP*, 2013, pp. 6108–6112.
- [20] X. Jia, M. Zhao, Y. Di, P. Li, and J. Lee, “Sparse filtering with the generalized ℓ_p/ℓ_q norm and its applications to the condition monitoring of rotating machinery,” *Mech. Syst. Signal Process.*, vol. 102, pp. 198–213, 2018.
- [21] Z. Zhou and J. Yu, “Sparse recovery based on q -ratio constrained minimal singular values,” *Signal Process.*, vol. 155, pp. 247–258, 2019.
- [22] C. Wang, M. Yan, Y. Rahimi, and Y. Lou, “Accelerated schemes for the L_1/L_2 minimization,” *IEEE Trans. Signal Process.*, vol. 68, pp. 2660–2669, 2020.
- [23] X. J. Chen, Z. S. Lu, and T. K. Pong, “Penalty methods for a class of non-lipschitz optimization problems,” *SIAM J. Optim.*, vol. 26, no. 3, pp. 1465–1492, 2016.
- [24] W. Hare and A. Lewis, “Identifying active constraints via partial smoothness and prox-regularity,” *J. Convex Anal.*, vol. 11, pp. 251–266, 2004.
- [25] S. Vaiter, M. Golbabaee, J. Fadili, and G. Peyré, “Model selection with low complexity priors,” *Inf. Inference*, vol. 4, no. 3, pp. 230–287, 2015.
- [26] J. Liang, J. Fadili, and G. Peyré, “Local linear convergence of forward–backward under partial smoothness,” in *NIPS*, Z. Ghahramani, M. Welling, C. Cortes, N. Lawrence, and K. Weinberger, Eds., vol. 27, 2014.
- [27] A. S. Lewis and S. J. Wright, “A proximal method for composite minimization,” *Math. Program.*, vol. 158, no. 5, pp. 501–546, 2016.
- [28] D. L. Donoho, “De-noising by soft-thresholding,” *IEEE Trans. Inf. Theory*, vol. 41, no. 3, pp. 613–627, 1995.
- [29] E. T. Hale, W. Yin, and Y. Zhang, “Fixed-point continuation for ℓ_1 -minimization: Methodology and convergence,” *SIAM J. Optim.*, vol. 19, no. 3, pp. 1107–1130, 2008.
- [30] J. V. Burke and J. J. More, “On the identification of active constraints,” *SIAM J. Numer. Anal.*, vol. 25, no. 5, pp. 1197–1211, 1988.
- [31] J. V. Burke, “On identification of active constraints II: the nonconvex case,” *SIAM J. Numer. Anal.*, vol. 27, pp. 1081–1102, 1990.
- [32] S. J. Wright, “Identifiable surfaces in constrained optimization,” *SIAM J. Control. Optim.*, vol. 31, no. 4, pp. 1063–1079, 1993.
- [33] A. Daniilidis, W. Hare, and J. Malick, “Geometrical interpretation of the predictor-corrector type algorithms in structured optimization problems,” *Optimization*, vol. 55, no. 5–6, pp. 481–503, 2006.
- [34] A. Daniilidis, D. Drusvyatskiy, and A. S. Lewis, “Orthogonal invariance and identifiability,” *SIAM J. Matrix Anal. Appl.*, vol. 35, no. 2, pp. 580–598, 2014.
- [35] S. Vaiter, G. Peyré, and J. Fadili, “Model consistency of partly smooth regularizers,” *IEEE Trans. Inf. Theory*, vol. 64, no. 3, pp. 1725–1737, 2018.
- [36] D. P. Bertsekas, “On the Goldstein-Levitin-Polyak gradient projection method,” *IEEE Trans. Autom. Control*, vol. 21, no. 2, pp. 174–184, 1976.
- [37] —, “Projected newton methods for optimization problems with simple constraints,” *SIAM J. Control. Optim.*, vol. 20, no. 2, pp. 221–246, 1982.
- [38] J. Liang, J. Fadili, and G. Peyré, “Activity identification and local linear convergence of forward–backward-type methods,” *SIAM J. Optim.*, vol. 27, no. 1, pp. 408–437, 2017.
- [39] A. S. Lewis, “Active sets, nonsmoothness, and sensitivity,” *SIAM J. Optim.*, vol. 13, no. 3, pp. 702–725, 2002.
- [40] P. Gong, C. Zhang, Z. Lu, J. Z. Huang, and J. Ye, “A general iterative shrinkage and thresholding algorithm for non-convex regularized optimization problems,” *PMLR*, vol. 28, no. 2, pp. 37–45, 2013.
- [41] H. Li and Z. Lin, “Accelerated proximal gradient methods for nonconvex programming,” in *NIPS*, C. Cortes, N. Lawrence, D. Lee, M. Sugiyama, and R. Garnett, Eds., vol. 28, 2015.
- [42] R. T. Rockafellar and R. J. B. Wets, *Variational analysis*.

- Springer Berlin, Heidelberg, 1998.
- [43] R. A. Poliquin and R. T. Rockafellar, “Prox-regular functions in variational analysis,” *Trans. Amer. Math. Soc.*, vol. 348, no. 5, pp. 1805–1838, 1996.
 - [44] R. Mifflin, “Semismooth and semiconvex functions in constrained optimization,” *SIAM J. Control. Optim.*, vol. 15, no. 6, pp. 959–972, 1977.
 - [45] F. Facchinei, “Minimization of SC^1 functions and the maratos effect,” *Operations Research Letters*, vol. 17, no. 3, pp. 131–137, 1995.
 - [46] F. H. Clarke, *Optimization and Nonsmooth Analysis*. Classical Appl. Math. Society for Industrial and Applied Mathematics, Philadelphia, PA, 1990, vol. 5.
 - [47] J. Li, A. M.-C. So, and W.-K. Ma, “Understanding notions of stationarity in nonsmooth optimization: A guided tour of various constructions of subdifferential for nonsmooth functions,” *IEEE Signal Proc. Mag.*, vol. 37, no. 5, pp. 18–31, 2020.
 - [48] J.-S. Pang, M. Razaviyayn, and A. Alvarado, “Computing B-stationary points of nonsmooth DC programs,” *Math. Oper. Res.*, vol. 42, no. 1, pp. 95–118, 2017.
 - [49] H. Qi and D. Sun, “A quadratically convergent newton method for computing the nearest correlation matrix,” *SIAM J. Matrix Anal. Appl.*, vol. 28, no. 2, pp. 360–385, 2006.
 - [50] X.-Y. Zhao, D. Sun, and K.-C. Toh, “A Newton-CG augmented lagrangian method for semidefinite programming,” *SIAM J. Optim.*, vol. 20, no. 4, pp. 1737–1765, 2010.
 - [51] E. D. Dolan and J. J. Moré, “Benchmarking optimization software with performance profiles,” *Math. Program.*, vol. 91, pp. 201–213, 2002.
 - [52] Z. Xu, X. Chang, F. Xu, and H. Zhang, “ $l_{1/2}$ regularization: a thresholding representation theory and a fast solver,” *IEEE Trans. Neural. Netw. Learn. Syst.*, vol. 23, no. 7, pp. 1013–1027, 2012.
 - [53] R. I. Boş, M. N. Dao, and G. Li, “Extrapolated proximal subgradient algorithms for nonconvex and nonsmooth fractional programs,” *Math. Oper. Res.*, vol. 47, no. 3, pp. 2415–2443, 2022.
 - [54] J. E. Dennis and R. B. Schnabel, *Numerical Methods for Unconstrained Optimization and Nonlinear Equations*. Society for Industrial and Applied Mathematics, 1996.

Supplementary Materials “On Partly Smoothness, Activity Identification and Faster Algorithms of L_1 over L_2 Minimization”

Min Tao and Xiao-Ping Zhang and Zi-Hao Xia

Definition S. 1. (Partly Smooth) [1, Definition 2.7] Suppose that the set $\mathcal{M} \subset \mathbb{R}^n$ contains the point \mathbf{x} . The function $f : \mathbb{R}^n \rightarrow \overline{\mathbb{R}}$ is partly smooth at \mathbf{x} relative to \mathcal{M} if \mathcal{M} is a manifold around \mathbf{x} and the following four properties hold:

- (i) (**Restricted Smoothness**) the restriction $f|_{\mathcal{M}}$ is smooth around \mathbf{x} ;
- (ii) (**Regularity**) at every point close to \mathbf{x} in \mathcal{M} , the function f is regular and has a subgradient;
- (iii) (**Normal Sharpness**) $df(\mathbf{x})(-\mathbf{w}) > -df(\mathbf{x})(\mathbf{w})$ for all nonzero directions \mathbf{w} in $N_{\mathcal{M}}(\mathbf{x})$;
- (iv) (**Subgradient Continuity**) the subdifferential map ∂f is continuous at \mathbf{x} relative to \mathcal{M} .

Definition S. 2. (Partly smooth sets) [1, Definition 2.8] A set $S \subset \mathbb{R}^n$ is partly smooth at a point \mathbf{x} relative to a set \mathcal{M} if ι_S is partly smooth at \mathbf{x} relative to \mathcal{M} . We say S is partly smooth relative to a set \mathcal{M} if \mathcal{M} is a manifold and S is partly smooth at each point in \mathcal{M} relative to \mathcal{M} .

The ensuing two concepts stem from the realm of sensitivity analysis, with the former serving as the foundation for the latter.

Definition S. 3. (strong local minimizer) [1, Definition 5.4] Given any subset \mathcal{M} of \mathbb{R}^n , a point \mathbf{x}_0 is a strong local minimizer of a function $f : \mathcal{M} \mapsto \overline{\mathbb{R}}$ if there exists a real $\delta > 0$ such that $f(\mathbf{x}) \geq f(\mathbf{x}_0) + \delta\|\mathbf{x} - \mathbf{x}_0\|^2$ for all $\mathbf{x} \in \mathcal{M}$ near \mathbf{x}_0 .

Definition S. 4. (strong critical point) [1, Definition 5.6] Suppose the function $f : \mathbb{R}^n \mapsto \overline{\mathbb{R}}$ is partly smooth at the point \mathbf{x}_0 relative to the set $\mathcal{M} \subset \mathcal{X}$. We call \mathbf{x}_0 a strong critical point of f relative to \mathcal{M} if

- (i) \mathbf{x}_0 is a strong local minimizer of $f|_{\mathcal{M}}$, and
- (ii) $0 \in \text{ri}\partial f(\mathbf{x}_0)$.

Assumption S. 1. For Euclidean spaces Y and Z , the set $Q \subset Y \times Z$ is a manifold containing the point $(\mathbf{y}_0, \mathbf{z}_0)$ and satisfies the condition

$$(\mathbf{w}, \mathbf{0}) \in N_Q(\mathbf{y}_0, \mathbf{z}_0) \Rightarrow \mathbf{w} = \mathbf{0},$$

where $N_Q(\mathbf{y}, \mathbf{z})$ is the normal space to Q at (\mathbf{y}, \mathbf{z}) . To proceed, we introduce several notions. For each vector $\mathbf{y} \in Y$, we define the set

$$Q_{\mathbf{y}} = \{\mathbf{z} \in Z | (\mathbf{y}, \mathbf{z}) \in Q\}.$$

Consider a function $p : Y \times Z \rightarrow \overline{\mathbb{R}}$, and we define a function $p_{\mathbf{y}} : Z \rightarrow \overline{\mathbb{R}}$ by $p_{\mathbf{y}}(\mathbf{z}) = p(\mathbf{y}, \mathbf{z})$ for $\mathbf{y} \in Y$ and $\mathbf{z} \in Z$. The subsequent theorem demonstrates that under certain conditions, strong criticality implies that the parametrized minimizer is also a strong critical point.

Theorem S. 1. [1, Theorem 5.7] Suppose Assumption S.1 holds and the function $p(\cdot)$ is partly smooth relative to the manifold Q . If the point \mathbf{z}_0 is a strong critical point of the function $p_{\mathbf{y}_0}(\cdot)$ relative to the set $Q_{\mathbf{y}_0}$, then there are open neighborhoods $U \subset Z$ of \mathbf{z}_0 and $V \subset Y$ of \mathbf{y}_0 and a continuously differentiable function $\Psi : V \mapsto U$ satisfying $\Psi(\mathbf{y}_0) = \mathbf{z}_0$ and for all $\mathbf{y} \in V$:

- (i) the function $p_{\mathbf{y}}|_{Q_{\mathbf{y}} \cap U}$ has a unique critical point $\Psi(\mathbf{y})$;
- (ii) $\Psi(\mathbf{y})$ is a strong critical point of the function $p_{\mathbf{y}}(\cdot)$ relative the manifold $Q_{\mathbf{y}} \cap U$.

The following lemma states that prox-regularity exactly ensures the well-definedness of the projection mapping. The term “prox-normal neighborhood” denotes the neighborhood \mathcal{V} of \mathcal{S} at $\bar{\mathbf{x}}$.

Lemma S. 2. [2, Lemma 2.2] Suppose the set $\mathcal{S} \in \mathbb{R}^m$ is closed. Then, \mathcal{S} is prox-regular at the point $\bar{\mathbf{x}} \in \mathcal{S}$ if and only if the projection mapping $P_{\mathcal{S}}$ is single value near $\bar{\mathbf{x}}$. In this case, there exists an open neighbourhood \mathcal{V} of $\bar{\mathbf{x}}$ on which the following properties hold:

- (i) $P_{\mathcal{S}}(\cdot)$ is single valued and Lipchitz continuous on \mathcal{V} .
- (ii) $P_{\mathcal{S}}(\cdot) = (I + N_{\mathcal{S}})^{-1}(\cdot)$ on \mathcal{V} .
- (iii) For any point \mathbf{x} and $\mathbf{v} \in \mathcal{V}$ such that $\mathbf{v} - \mathbf{x} \in N_{\mathcal{S}}(\mathbf{x})$ implies that $\mathbf{x} = P_{\mathcal{S}}(\mathbf{v})$.

Below, we first prove the following lemma.

Lemma S. 3. *If \mathcal{M} is prox-regular at $\bar{\mathbf{x}} \in \mathcal{M}$, the normal vector $\bar{\mathbf{y}} - \bar{\mathbf{x}} \in N_{\mathcal{M}}(\bar{\mathbf{x}})$ is sufficiently small such that $2(\bar{\mathbf{y}} - \bar{\mathbf{x}})$ in the “prox-normal neighborhood” of \mathcal{M} , then*

$$\mathbf{x} \in \mathcal{M} \Rightarrow \|\mathbf{x} - \bar{\mathbf{y}}\|^2 \geq \|\bar{\mathbf{x}} - \bar{\mathbf{y}}\|^2 + \frac{1}{2}\|\mathbf{x} - \bar{\mathbf{x}}\|^2.$$

Proof. Since $\|\mathbf{x} - \bar{\mathbf{y}}\|^2 = \|\mathbf{x} - \bar{\mathbf{x}}\|^2 + \|\bar{\mathbf{x}} - \bar{\mathbf{y}}\|^2 + 2\langle \mathbf{x} - \bar{\mathbf{x}}, \bar{\mathbf{x}} - \bar{\mathbf{y}} \rangle$, we only need to verify that

$$\|\mathbf{x} - \bar{\mathbf{x}} + 2(\bar{\mathbf{x}} - \bar{\mathbf{y}})\|^2 \geq \|2(\bar{\mathbf{x}} - \bar{\mathbf{y}})\|^2. \quad (\text{S.1})$$

Since \mathcal{M} is prox-regular at $\bar{\mathbf{x}}$, we choose sufficiently small normal vector $2(\bar{\mathbf{y}} - \bar{\mathbf{x}})$ such that it is in the “prox-normal neighborhood” of \mathcal{M} at $\bar{\mathbf{x}}$. It leads to $P_{\mathcal{M}}[\bar{\mathbf{x}} + 2(\bar{\mathbf{y}} - \bar{\mathbf{x}})] = \bar{\mathbf{x}}$ due to Lemma S. 2 (iii). Furthermore,

$$\begin{aligned} \|\mathbf{x} - \bar{\mathbf{x}} + 2(\bar{\mathbf{x}} - \bar{\mathbf{y}})\|^2 &\geq \min\{\|\mathbf{x} - (\bar{\mathbf{x}} + 2(\bar{\mathbf{y}} - \bar{\mathbf{x}}))\|^2 | \mathbf{x} \in \mathcal{M}\} \\ &= \|P_{\mathcal{M}}(\bar{\mathbf{x}} + 2(\bar{\mathbf{y}} - \bar{\mathbf{x}})) - (\bar{\mathbf{x}} + 2(\bar{\mathbf{y}} - \bar{\mathbf{x}}))\|^2 \\ &= \|2(\bar{\mathbf{y}} - \bar{\mathbf{x}})\|^2. \end{aligned}$$

Thus, (S.1) holds. The conclusion follows directly. \square

The following theorem relax the condition in [2, Theorem 3.3] of “the set \mathcal{S} is \mathcal{C}^p -partly smooth ($p \geq 2$)” to “the set \mathcal{S} is partly smooth (i.e., $\iota_{\mathcal{S}}$ be \mathcal{C}^1)” (see Definition S.2).

Theorem S. 4. *Let the set \mathcal{S} be prox-regular and partly smooth at the point $\bar{\mathbf{x}}$ relative to \mathcal{M} . For any sufficiently small normal vector $\bar{\mathbf{n}} := \bar{\mathbf{y}} - \bar{\mathbf{x}} \in \text{ri}N_{\mathcal{S}}(\bar{\mathbf{x}})$ ($\bar{\mathbf{n}}$ in prox-normal neighbourhood), there exists a neighbourhood V of $(\bar{\mathbf{x}} + \bar{\mathbf{n}})$ on which the projection mappings satisfy $P_{\mathcal{S}} = P_{\mathcal{M}}$ on V .*

Proof. Define the function ρ

$$\begin{aligned} \rho : \mathbb{R}^m \times \mathbb{R}^m &\mapsto \overline{\mathbb{R}} \\ (\mathbf{n}, \mathbf{x}) &\mapsto \frac{1}{2}\|\mathbf{x} - \mathbf{n} - \bar{\mathbf{x}}\|^2 + \iota_{\mathcal{S}}(\mathbf{x}). \end{aligned}$$

We claim that Assumption S. 1 holds with $Y = Z = \mathbb{R}^m$, $Q = \mathbb{R}^m \times \mathcal{M}$ and $(\mathbf{y}_0, \mathbf{z}_0) = (\bar{\mathbf{n}}, \bar{\mathbf{x}})$. By noting that

$$(\mathbf{n}, \mathbf{0}) \in N_Q(\bar{\mathbf{n}}, \bar{\mathbf{x}}) \Rightarrow \mathbf{n} = \mathbf{0}.$$

Second, $\rho(\mathbf{n}, \mathbf{x})$ is partly smooth at $(\bar{\mathbf{n}}, \bar{\mathbf{x}})$ relative to $\mathbb{R}^m \times \mathcal{M}$ since the set \mathcal{S} is partly smooth at the point $\bar{\mathbf{x}}$ relative to \mathcal{M} . Since $\partial\rho_{\bar{\mathbf{n}}}(\bar{\mathbf{x}}) = -\bar{\mathbf{n}} + N_{\mathcal{S}}(\bar{\mathbf{x}})$ and $\bar{\mathbf{n}} \in \text{ri}N_{\mathcal{S}}(\bar{\mathbf{x}})$, it ensures that $0 \in \text{ri}\partial\rho_{\bar{\mathbf{n}}}(\bar{\mathbf{x}})$. On the other hand, we have the following inequality

$$\mathbf{x} \in \mathcal{M} \text{ and } \mathbf{x} \text{ near } \bar{\mathbf{x}} \Rightarrow \frac{1}{2}\|\mathbf{x} - \bar{\mathbf{n}} - \bar{\mathbf{x}}\|^2 \geq \frac{1}{2}\|\bar{\mathbf{n}}\|^2 + \frac{1}{4}\|\mathbf{x} - \bar{\mathbf{x}}\|^2,$$

due to Lemma S. 3. It implies that $\bar{\mathbf{x}}$ is a strong critical point of $\rho_{\bar{\mathbf{n}}}(\cdot)$ (setting $\delta = 1/4$ in Definition S. 3). Then, using Theorem S. 1, there exists a mapping $\psi : \mathbb{R}^m \rightarrow \mathcal{M}$ such that $\psi(\bar{\mathbf{n}}) = \bar{\mathbf{x}}$ and $\psi(\mathbf{n})$ is a strong critical point of $\rho_{\mathbf{n}}(\cdot)$ relative to \mathcal{M} near $\bar{\mathbf{x}}$. It implies that $0 \in \text{ri}\partial\rho_{\mathbf{n}}(\psi(\mathbf{n}))$. It further leads to $\mathbf{n} + \bar{\mathbf{x}} - \psi(\mathbf{n}) \in \text{ri}N_{\mathcal{S}}(\psi(\mathbf{n}))$. $P_{\mathcal{S}}(\mathbf{n} + \bar{\mathbf{x}}) = \psi(\mathbf{n}) = P_{\mathcal{M}}(\mathbf{n} + \bar{\mathbf{x}})$ due to $\psi(\mathbf{n}) \in \mathcal{M}$. \square

Based on Theorem S. 4, we can further prove the following result which we relax the condition in [2, Theorem 4.1] of “the set \mathcal{S} is \mathcal{C}^p -partly smooth ($p \geq 2$)” to “the set \mathcal{S} is partly smooth (i.e., $\iota_{\mathcal{S}}$ be \mathcal{C}^1)” (see Definition S.2).

Theorem S. 5. *Consider a set \mathcal{S} be partly smooth at the point $\bar{\mathbf{x}}$ relative the manifold \mathcal{M} , and prox-regular there. If the normal vector $\bar{\mathbf{n}}$ is in $\text{ri}N_{\mathcal{S}}(\bar{\mathbf{x}})$ and the sequence $\{\mathbf{x}_k\}$ and $\{\mathbf{d}_k\}$ satisfy*

$$\mathbf{x}_k \rightarrow \bar{\mathbf{x}}, \mathbf{d}_k \rightarrow \bar{\mathbf{n}}, \text{ and } \text{dist}(\mathbf{d}_k, N_{\mathcal{S}}(\mathbf{x}_k)) \rightarrow 0,$$

then

$$\mathbf{x}_k \in \mathcal{M} \text{ for all large } k.$$

Proof. The proof follows the routines of [2, Theorem 4.1] by using Lemma S. 2 and Theorem S. 4. \square

The following theorem relax the condition in [2, Theorem 4.3] of “the set \mathcal{S} is \mathcal{C}^p -partly smooth ($p \geq 2$)” to “the set \mathcal{S} is partly smooth (i.e., $\iota_{\mathcal{S}}$ be \mathcal{C}^1)” (see Definition S.2).

Theorem S. 6. *Consider a \mathcal{C}^1 function f . Let the set \mathcal{S} be partly smooth at the point $\bar{\mathbf{x}}$ relative the manifold \mathcal{M} , and prox-regular there. Suppose $\mathbf{x}_k \rightarrow \bar{\mathbf{x}}$ and $-\nabla f(\bar{\mathbf{x}}) \in \text{ri}N_{\mathcal{S}}(\bar{\mathbf{x}})$. Then, $\mathbf{x}_k \in \mathcal{M}$ for all large k if and only if $\text{dist}(-\nabla f(\mathbf{x}_k), N_{\mathcal{S}}(\mathbf{x}_k)) \rightarrow 0$.*

Proof. The proof follows the routines of [2, Theorem 4.3] by using Theorem S. 5 for the “sufficient direction”. \square

Now, we are in the stage to conclude the main result. The following theorem relaxes the condition in [2, Theorem 5.3] of “the function f be C^p -partly smooth ($p \geq 2$)” to “the function f be partly smooth (i.e., f be C^1)”.

Theorem S. 7. *Let the function f be partly smooth at the point $\bar{\mathbf{x}}$ relative to the manifold \mathcal{M} , and prox-regular there, with $\mathbf{0} \in \text{ri}\partial f(\bar{\mathbf{x}})$. Suppose $\mathbf{x}_k \rightarrow \bar{\mathbf{x}}$ and $f(\mathbf{x}_k) \rightarrow f(\bar{\mathbf{x}})$. Then,*

$$\mathbf{x}_k \in \mathcal{M} \text{ for all large } k$$

if and only if

$$\text{dist}(\mathbf{0}, \partial f(\mathbf{x}_k)) \rightarrow 0.$$

Proof. First, we show that if f is partly smooth at a point $\bar{\mathbf{x}}$ relative to a manifold \mathcal{M} , $\text{epi}f$ is partly smooth at $\bar{\mathbf{z}} = (\bar{\mathbf{x}}, f(\bar{\mathbf{x}}))$ relative to the manifold $\widehat{\mathcal{M}} = \{(\mathbf{x}, f(\mathbf{x})) : \mathbf{x} \in \mathcal{M}\}$. We define

$$\begin{aligned} h : \mathbb{R}^{m+1} &\mapsto \mathbb{R} \\ (\mathbf{x}, r) &\mapsto f(\Phi(\mathbf{x}, r)) - r, \end{aligned}$$

where the function $\Phi(\mathbf{x}, r) = \mathbf{x}$. Thus, $\text{epi}f = \{(\mathbf{x}, r) | f(\Phi(\mathbf{x}, r)) - r \leq 0\}$. Applying the chain rule [1], sum rule [1] and level set rule [1], we show that $\text{epi}f$ is partly smooth at $(\bar{\mathbf{x}}, f(\bar{\mathbf{x}}))$ relative to the manifold $\widehat{\mathcal{M}}$. To show the chain rule [1, Theorem 4.2] applicable, we only need to check Φ is transversal to \mathcal{M} , i.e.,

$$\text{Ker}(\nabla\Phi(\mathbf{z})^*) \cap N_{\mathcal{M}}(\Phi(\mathbf{z})) = \{\mathbf{0}\},$$

where $\mathbf{z} = (\mathbf{x}, r)$. Since $(\nabla\Phi(\mathbf{z}))^* = \begin{pmatrix} I_m \\ \mathbf{0}_{1 \times m} \end{pmatrix}$, then $\text{Ker}(\nabla\Phi(\mathbf{z})^*) = \{\mathbf{0}\}$. Thus, the chain rule holds. Therefore, $\text{epi}f$ is partly smooth at $(\bar{\mathbf{x}}, f(\bar{\mathbf{x}}))$ relative to the manifold $\widehat{\mathcal{M}}$ from that f is partly smooth at a point $\bar{\mathbf{x}}$ relative to a manifold \mathcal{M} . Second, using [3, Theorem 3.5], $\text{epi}f$ is prox-regularity at $\bar{\mathbf{z}}$. Define $\mathcal{S} = \text{epi}f$, and define

$$\begin{aligned} \varphi : \mathbb{R}^m \times \mathbb{R} &\mapsto \mathbb{R} \\ (\mathbf{x}, r) &\mapsto r. \end{aligned}$$

Let $\mathbf{z}_k = (\mathbf{x}_k, f(\mathbf{x}_k))$ and $-\nabla\varphi(\bar{\mathbf{z}}) = (\mathbf{0}, -1) \in \text{ri}N_{\mathcal{S}}(\bar{\mathbf{z}})$. Then, it follows from Theorem S. 6, we have

$$\begin{aligned} &\mathbf{x}_k \in \mathcal{M} \text{ for all large } k \\ &\Leftrightarrow \mathbf{z}_k \in \widehat{\mathcal{M}} \text{ for all large } k \\ &\Leftrightarrow \text{dist}(-\nabla\varphi(\mathbf{z}_k), N_{\mathcal{S}}(\mathbf{x}_k, f(\mathbf{x}_k))) \rightarrow 0 \\ &\Leftrightarrow \text{dist}((\mathbf{0}, -1), N_{\mathcal{S}}(\mathbf{x}_k, f(\mathbf{x}_k))) \rightarrow 0 \\ &\Leftrightarrow \text{dist}(\mathbf{0}, \partial f(\mathbf{x}_k)) \rightarrow 0. \end{aligned}$$

□

REFERENCES

- [1] A. S. Lewis, “Active sets, nonsmoothness, and sensitivity,” *SIAM J. Optim.*, vol. 13, no. 3, pp. 702–725, 2002.
- [2] W. Hare and A. Lewis, “Identifying active constraints via partial smoothness and prox-regularity,” *J. Convex Anal.*, vol. 11, pp. 251–266, 2004.
- [3] R. A. Poliquin and R. T. Rockafellar, “Prox-regular functions in variational analysis,” *Trans. Amer. Math. Soc.*, vol. 348, no. 5, pp. 1805–1838, 1996.